

Flexible Bayesian Dynamic Modeling of Correlation and Covariance Matrices

BY SHIWEI LAN

*Department of Statistics, University of Illinois Urbana-Champaign, Champaign, IL 61820,
USA*

ANDREW HOLBROOK

Department of Statistics, University of California-Irvine, Irvine, CA 92697, USA

GABRIEL A. ELIAS AND NORBERT J. FORTIN

*Center for the Neurobiology of Learning and Memory, Department of Neurobiology and
Behavior, University of California-Irvine, Irvine, CA 92697, USA*

HERNANDO OMBAO

*Department of Statistics, University of California-Irvine, Irvine, CA 92697, USA
Statistics Program, King Abdullah University of Science and Technology, Thuwal 23955, Saudi
Arabia*

BABAK SHAHBABA

Department of Statistics, University of California-Irvine, Irvine, CA 92697, USA

SUMMARY

Modeling correlation (and covariance) matrices can be challenging due to the positive-definiteness constraint and potential high-dimensionality. Our approach is to decompose the covariance matrix into the correlation and variance matrices and propose a novel Bayesian framework based on modeling the correlations as products of unit vectors. By specifying a wide range of distributions on a sphere (e.g. the squared-Dirichlet distribution), the proposed approach induces flexible prior distributions for covariance matrices (that go beyond the commonly used inverse-Wishart prior). For modeling real-life spatio-temporal processes with complex dependence structures, we extend our method to dynamic cases and introduce unit-vector Gaussian process priors in order to capture the evolution of correlation among multiple time series. To handle the intractability of the resulting posterior, we introduce the adaptive Δ -Spherical Hamiltonian Monte Carlo. Using an example of normal-Inverse-Wishart problem, a simulated periodic process, and an analysis of local field potential activity data (collected from the hippocampus of rats performing a complex sequence memory task), we demonstrate the validity and effectiveness of our proposed framework for (dynamic) modeling covariance and correlation matrices.

Some key words: Dynamic covariance modeling, Spatio-temporal models, Geometric methods, Posterior contraction, Δ -Spherical Hamiltonian Monte Carlo.

1. INTRODUCTION

Modeling covariance matrices—or more broadly, positive definite (PD) matrices—is one of the most fundamental problems in statistics. In general, the task is difficult because the number of parameters grows quadratically with the dimension of the matrices. The complexity of the challenge increases substantially if we allow dependencies to vary over time (or space) in order to account for the dynamic (non-stationary) nature of the underlying probability model. In this paper, we propose a novel solution to the problem by developing a flexible and yet computationally efficient inferential framework for both fixed and dynamic covariance matrices.

Within the Bayesian framework, it is common to use an inverse-Wishart prior on the covariance matrix for computational convenience (Mardia et al., 1980; Anderson, 2003). This choice of prior however is very restrictive (e.g. common degrees of freedom for all components of variance) (Barnard et al., 2000; Tokuda et al., 2011). Daniels (1999); Daniels & Kass (2001) propose uniform shrinkage priors. Daniels & Kass (1999) discuss three hierarchical priors to generalize the inverse-Wishart prior. Alternatively, one may use decomposition strategies for more flexible modeling choices (Barnard et al., 2000). For instance, Banfield & Raftery (1993), Yang & Berger (1994), Celeux & Govaert (1995), Leonard & Hsu (1992), Chiu et al. (1996), and Bensmail et al. (1997) propose methods based on the spectral decomposition of the covariance matrix. Another strategy is to use the Cholesky decomposition of the covariance matrix or its inverse, e.g., Pourahmadi (1999, 2000); Liu (1993); Pinheiro & Bates (1996). There are other approaches directly related to correlation, including the constrained model based on truncated distributions (Liechty, 2004), the Cholesky decomposition of correlation matrix using an angular parametrization (Pourahmadi & Wang, 2015), and methods based on partial autocorrelation and parameterizations using angles (Rapisarda et al., 2007). In general, these methods fail to yield full flexibility and generality; and often sacrifice statistical interpretability.

While our proposed method in this paper is also based on the separation strategy (Barnard et al., 2000) and the Cholesky decomposition, unlike the existing methods it represents each entry of the correlation matrix as a product of unit vectors. This in turn provides a flexible framework for modeling covariance matrices without sacrificing interpretability. Additionally, this framework can be easily extended to dynamic settings in order to model real-life spatio-temporal processes with complex dependence structures (e.g., brain signals during cognitive tasks). This proposed model has the potential impact to model dynamic brain connectivity. A number of new methods have been developed (Cribben et al., 2012; Fiecas & Ombao, 2016; Lindquist et al., 2014; Ting et al., 2015; Prado, 2013) for brain connectivity analyses. One advantage of this model is that it provides both a nonparametric Bayesian model and an efficient inferential method for modeling the complex dynamic dependence among multiple stochastic processes that is common in the study of brain activity.

To address the constraint for correlation processes (positive definite matrix at each time having unit diagonals and off-diagonal entries with magnitudes no greater than 1), we introduce unit-vector Gaussian process priors. There are other related works, e.g. generalized Wishart process (Wilson & Ghahramani, 2011), and latent factor process (Fox & Dunson, 2015), that explore the product of vector Gaussian processes. In general they do not grant full flexibility in simultaneously modeling the mean, variance and correlation processes. For example, latent factor based models link the mean and covariance processes through a loading matrix, which is restrictive and undesirable if the linear link is not appropriate, and thus are outperformed by our proposed flexible framework (See more details in Section 4.2). Other approaches to model non-stationary processes use a representation in terms of a basis such as wavelets (Nason et al., 2000; Park et al., 2014; Cho & Fryzlewicz, 2015) and the SLEX (Ombao et al., 2005), which are actually

inspired by the Fourier representations in the Dahlhaus locally stationary processes (Dahlhaus, 2000; Priestley, 1965). These approaches are frequentist and do not easily provide a framework for inference (e.g., obtaining confidence intervals).

This main contributions of this paper are: (a.) a sphere-product representation of correlation/covariance matrix is introduced to induce flexible priors for correlation/covariance matrices and processes; (b.) a general and flexible framework is proposed for modeling mean, variance, and correlation processes separately; (c.) an efficient algorithm is introduced to infer correlation matrices and processes; (d.) posterior contraction phenomena are studied for both mean and covariance (correlation) processes.

The rest of the paper is organized as follows. In the next section, we present a geometric view of covariance matrices and extend this view to allow covariance matrices to change over time. In Section 3, we use this geometrical perspective to develop an effective and computationally efficient inferential method for modeling static and dynamic covariance matrices. Using simulated data, we will evaluate our method in Section 4. In Section 5, we apply our proposed method to local field potential (LFP) data recorded from the hippocampus of rats performing a complex sequence memory task. In the final section, we conclude with discussions about future work.

2. STRUCTURED BAYESIAN MODELING OF COVARIANCE (CORRELATION)

To derive flexible models for covariance and correlation matrices, we start with the Cholesky decomposition of covariance, form a sphere-product representation, and finally obtain the separation decomposition in Barnard et al. (2000) with correlations represented as products of unit vectors. The sphere-product representation is amenable for the inferential algorithm to handle the resulting intractability, and hence lays the foundation for full flexibility in choosing priors.

Any covariance matrix $\Sigma = [\sigma_{ij}] > 0$ is symmetric positive definite, and hence has a unique Cholesky decomposition $\Sigma = \mathbf{L}\mathbf{L}^\top$ where the Cholesky factor $\mathbf{L} = [l_{ij}]$ is a lower triangular matrix such that $\sigma_{ij} = \sum_{k=1}^{\min\{i,j\}} l_{ik}l_{jk}$. Then each variance $\sigma_i^2 := \sigma_{ii}$ can be written in terms of the corresponding row $\mathbf{l}_i := [l_{i1}, l_{i2}, \dots, l_{ii}]$ of \mathbf{L} , i.e. $\sigma_i^2 = \sum_{k=1}^i l_{ik}^2 = \|\mathbf{l}_i\|^2$. For $\Sigma > 0$, it is equivalent to require all the leading principal minors $\{M_i\}$ to be positive:

$$M_i = \prod_{k=1}^i l_{kk}^2 > 0, \quad i = 1, \dots, D \iff l_{ii} \neq 0, \quad i = 1, \dots, D$$

Based on this observation, for $i \in \{1, \dots, D\}$, \mathbf{l}_i can be viewed as a point on a sphere with radius σ_i excluding the equator, denoted as $\mathcal{S}_0^{i-1}(\sigma_i) := \{\mathbf{l} \in \mathbb{R}^i \mid \|\mathbf{l}\|_2 = \sigma_i, l_{ii} \neq 0\}$. Therefore the space of the Cholesky factor in terms of its rows can be written as a product of spheres. Note

$$(\mathbf{l}_1, \mathbf{l}_2, \dots, \mathbf{l}_D) = (l_{11}, l_{21}, l_{22}, \dots, l_{D1}, \dots, l_{DD}) \in \mathcal{S}_0^0(\sigma_1) \times \mathcal{S}_0^1(\sigma_2) \cdots \times \mathcal{S}_0^{D-1}(\sigma_D) \quad (1)$$

is the sufficient and necessary condition for $\Sigma = \mathbf{L}\mathbf{L}^\top$ to be a covariance matrix.

We present probabilistic models involving covariance matrices in the following generic form:

$$\begin{aligned} \mathbf{y} \mid \Sigma(\boldsymbol{\sigma}, \mathbf{L}) &\sim \ell(\mathbf{y}; \Sigma(\boldsymbol{\sigma}, \mathbf{L})), \quad \Sigma(\boldsymbol{\sigma}, \mathbf{L}) = \mathbf{L}\mathbf{L}^\top \\ \boldsymbol{\sigma} &\sim p(\boldsymbol{\sigma}) \\ \mathbf{L} \mid \boldsymbol{\sigma} &\sim p(\mathbf{L}; \boldsymbol{\sigma}), \quad \text{vech}^\top(\mathbf{L}) \in \prod_{i=1}^D \mathcal{S}_0^{i-1}(\sigma_i) \end{aligned} \quad (2)$$

where $\boldsymbol{\sigma} := [\sigma_1, \dots, \sigma_D]^\top$, and the half-vectorization in row order, vech^\top , transforms the lower triangular matrix \mathbf{L} into a vector $(\mathbf{l}_1, \mathbf{l}_2, \dots, \mathbf{l}_D)$. The total dimension of $(\boldsymbol{\sigma}, \mathbf{L})$ is $\frac{D(D+1)}{2}$.¹

Alternatively, we can make use of the *separation strategy* (Barnard et al., 2000) to decompose covariances in terms of standard deviations and correlations: $\boldsymbol{\Sigma} = \text{diag}(\boldsymbol{\sigma})\mathbf{P}\text{diag}(\boldsymbol{\sigma})$. Then we have a unique Cholesky decomposition for the correlation matrix $\mathbf{P} = [\rho_{ij}] = \mathbf{L}^*(\mathbf{L}^*)^\top$, where the Cholesky factor $\mathbf{L}^* = \text{diag}(\boldsymbol{\sigma}^{-1})\mathbf{L}$ can be obtained by normalizing each row of \mathbf{L} . The magnitude requirements for correlations are immediately satisfied by the Cauchy-Schwarz inequality: $|\rho_{ij}| = \frac{|\sigma_{ij}|}{\sigma_i\sigma_j} = \frac{|\langle \mathbf{l}_i, \mathbf{l}_j \rangle|}{\|\mathbf{l}_i\|_2\|\mathbf{l}_j\|_2} \leq 1$. Thus we require

$$(\mathbf{I}_1^*, \mathbf{I}_2^*, \dots, \mathbf{I}_D^*) \in \mathcal{S}_0^0 \times \mathcal{S}_0^1 \cdots \times \mathcal{S}_0^{D-1} \quad (3)$$

where $\mathcal{S}_0^{i-1} := \mathcal{S}_0^{i-1}(1)$. Similarly, (3) is the sufficient and necessary condition for $\mathbf{P} = \mathbf{L}^*(\mathbf{L}^*)^\top$ to be a correlation matrix. Then we have the following alternative structured model

$$\begin{aligned} \mathbf{y} | \boldsymbol{\Sigma}(\boldsymbol{\sigma}, \mathbf{L}^*) &\sim \ell(\mathbf{y}; \boldsymbol{\Sigma}(\boldsymbol{\sigma}, \mathbf{L}^*)), \quad \boldsymbol{\Sigma}(\boldsymbol{\sigma}, \mathbf{L}^*) = \text{diag}(\boldsymbol{\sigma})\mathbf{P}\text{diag}(\boldsymbol{\sigma}), \quad \mathbf{P} = \mathbf{L}^*(\mathbf{L}^*)^\top \\ \boldsymbol{\sigma} &\sim p(\boldsymbol{\sigma}) \\ \mathbf{L}^* &\sim p(\mathbf{L}^*), \quad \text{vech}^\top(\mathbf{L}^*) \in \prod_{i=1}^D \mathcal{S}_0^{i-1} \end{aligned} \quad (4)$$

In what follows, we will show that the above framework includes the inverse-Wishart prior as a special case, but it can be easily generalized to a broader range of priors for additional flexibility. Such flexibility enables us to better express prior knowledge, control the model complexity and speed up computation in modeling real-life phenomena.

2.1. Connection to the Inverse-Wishart Prior

There are some interesting connections between the spherical product representations (1) (3) and the early development of the Wishart distribution (Wishart, 1928). The original Wishart distribution was derived by orthogonalizing multivariate Gaussian random variables (See more details in Sverdrup, 1947; Anderson, 2003).

Suppose $\boldsymbol{\Sigma}$ is a random sample from the inverse-Wishart distribution $\mathcal{W}_D^{-1}(\boldsymbol{\Psi}, \nu)$ with the scale matrix $\boldsymbol{\Psi} > 0$ and the degree of freedom $\nu \geq D$. Therefore, $\boldsymbol{\Sigma}^{-1} \sim \mathcal{W}_D(\boldsymbol{\Psi}^{-1}, \nu)$. Denote \mathbf{C} as the Cholesky factor of $\boldsymbol{\Psi}^{-1}$, i.e. $\boldsymbol{\Psi}^{-1} = \mathbf{C}\mathbf{C}^\top$. Then $\boldsymbol{\Sigma}^{-1}$ has the following Bartlett decomposition (Anderson, 2003; Smith & Hocking, 1972)

$$\boldsymbol{\Sigma}^{-1} = \mathbf{T}\mathbf{T}^\top, \quad \mathbf{T} := \mathbf{C}\mathbf{T}^*, \quad t_{ij}^* \sim \begin{cases} \chi_{D-i+1}, & i = j \\ \mathcal{N}(0, 1), & i > j \\ \delta_0, & i < j \end{cases} \quad (5)$$

where the *Bartlett factor*, \mathbf{T} , is a lower triangular matrix. Now taking the inverse of the first equation in (5) yields the *reversed Cholesky decomposition*² $\boldsymbol{\Sigma} = \mathbf{U}\mathbf{U}^\top$, where $\mathbf{U} := \mathbf{T}^{-\top}$ is an upper triangular matrix. The following theorem describes the density of \mathbf{U} , which enables us to treat the inverse-Wishart distribution as a special instance of strategy (2) or (4).

¹ For each $i \in \{1, \dots, D\}$, given σ_i , there are only $(i-1)$ free parameters on $\mathcal{S}_0^{i-1}(\sigma_i)$, so there are totally $\frac{D(D-1)}{2} + D$ free parameters.

² This can be achieved through the *exchange matrix* (a.k.a. reversal matrix, backward identity, or standard involutory permutation) \mathbf{E} with 1's on the anti-diagonal and 0's elsewhere. Note that \mathbf{E} is both involutory and orthogonal, i.e. $\mathbf{E} = \mathbf{E}^{-1} = \mathbf{E}^\top$. Let $\mathbf{E}\boldsymbol{\Sigma}\mathbf{E} = \mathbf{L}\mathbf{L}^\top$ be the usual Cholesky decomposition. Then $\boldsymbol{\Sigma} = (\mathbf{E}\mathbf{L}\mathbf{E})(\mathbf{E}\mathbf{L}\mathbf{E})^\top = \mathbf{U}\mathbf{U}^\top$ and define $\mathbf{U} := \mathbf{E}\mathbf{L}\mathbf{E}^\top$.

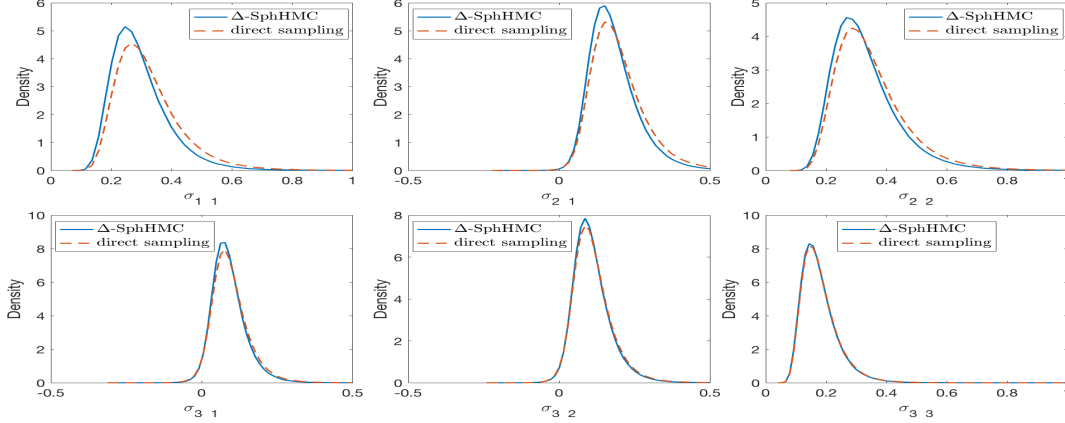


Fig. 1: Marginal posterior densities of σ_{ij} in the normal-inverse-Wishart problem. Solid blue lines are estimates by Δ -SphHMC and dashed red lines are estimates by direct sampling.

THEOREM 1. Assume $\Sigma \sim \mathcal{W}_D^{-1}(\Psi, \nu)$. Then its reversed Cholesky factor \mathbf{U} has the following density

$$p(\mathbf{U}) = \frac{|\Psi|^{\nu/2}}{2^{D(\nu-2)/2} \Gamma_D(\nu/2)} |\mathbf{U}|^{-(\nu+D+1)} \prod_{i=1}^D u_{ii}^i \exp\left(-\frac{1}{2} \text{tr}(\Psi \mathbf{U}^{-\top} \mathbf{U}^{-1})\right)$$

Proof. See Section A in the supplementary file. \square

If we normalize each row of $\mathbf{U} = \text{diag}(\boldsymbol{\sigma}) \mathbf{U}^*$ and write $u_{ij}^* = u_{ij}/\sigma_i$ with $\sigma_i = \|\mathbf{u}_i\|$, then the following joint prior of $(\boldsymbol{\sigma}, \mathbf{U}^*)$ is inseparable in general:

$$p(\boldsymbol{\sigma}, \mathbf{U}^*) \propto \prod_{i=1}^D |\sigma_i u_{ii}^*|^{i-(\nu+D+1)} \exp\left\{-\frac{1}{2} \text{tr}(\Psi \text{diag}(\boldsymbol{\sigma}^{-1})(\mathbf{U}^*)^{-\top} (\mathbf{U}^*)^{-1} \text{diag}(\boldsymbol{\sigma}^{-1}))\right\} \quad (6)$$

However, we can conditionally model variance and correlation factor as $p(\boldsymbol{\sigma}|\mathbf{U}^*)$ and $p(\mathbf{U}^*|\boldsymbol{\sigma})$ respectively, similarly as in our proposed scheme (2) or (4). Figure 1 verifies the validity of our proposed method (4) by showing that marginal densities of entries in Σ estimated from MCMC samples obtained by such conditional construction closely match the corresponding results by direct sampling in a normal-inverse-Wishart example (Section 4.1). This representation facilitates the construction of more flexible prior distributions for covariance matrix detailed below.

2.2. More Flexible Priors

Since $\boldsymbol{\sigma}$ and \mathbf{L}^* have independent priors in (4), in what follows we mainly focus on the scheme (4), and for simplicity, we denote the normalized Cholesky factor as \mathbf{L} . Also, following Barnard et al. (2000), we assume a log-Normal prior on $\boldsymbol{\sigma}$: $\log(\boldsymbol{\sigma}) \sim \mathcal{N}(\boldsymbol{\xi}, \boldsymbol{\Lambda})$.

The spherical product representation in (4) enables us to develop a broader class of priors on correlation. If two variables, y_i and y_j (assuming $i < j$) are known to be uncorrelated a priori, i.e. $0 = \rho_{ij} = \langle \mathbf{l}_i, \mathbf{l}_j \rangle$, then we can choose a prior that encourages $\mathbf{l}_i \perp \mathbf{l}_j$, e.g. $l_{jk} \approx 0$ for $k \leq i$. In contrast, if we believe a priori that there is a strong correlation between the two variables, we can specify that \mathbf{l}_i and \mathbf{l}_j be linearly dependent, e.g., by setting $[l_{jk}]_{k \leq i} \approx \pm \mathbf{l}_i$. Putting more prior probability on the diagonal elements of \mathbf{L} renders fewer non-zero off-diagonal elements,

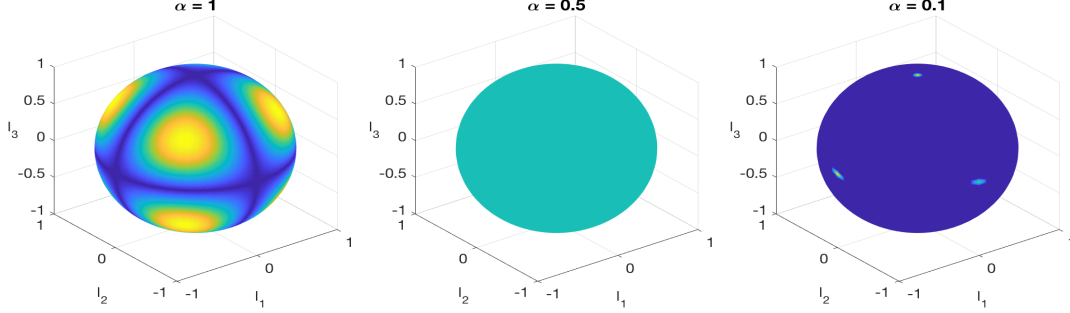


Fig. 2: Symmetric squared-Dirichlet distributions $\text{Dir}^2(\boldsymbol{\alpha})$ defined on the 2-sphere with different settings for concentration parameter $\boldsymbol{\alpha} = \alpha \mathbf{1}$. The uniform distribution on the simplex, $\text{Dir}(\mathbf{1})$, becomes non-uniform on the sphere due to the stretch of geometry (left); the symmetric Dirichlet distribution $\text{Dir}(\frac{1}{2}\mathbf{1})$ becomes uniform on the sphere (middle); with α closer to 0, the induced distribution becomes more concentrated on the polar points (right).

which in turn leads to a larger number of perpendicular rows; that is, such a prior favors zeros in the correlation matrix \mathbf{P} . More generally, one can map a probability distribution defined on the simplex onto the sphere and consider the following *squared-Dirichlet* distribution.

Definition 1 (Squared-Dirichlet distribution). A random vector $\mathbf{l}_i \in \mathcal{S}^{i-1}$ is said to have a *squared-Dirichlet* distribution with parameter $\boldsymbol{\alpha}_i := (\alpha_{i1}, \alpha_{i2}, \dots, \alpha_{ii})$ if

$$\mathbf{l}_i^2 := (l_{i1}^2, l_{i2}^2, \dots, l_{ii}^2) \sim \text{Dir}(\boldsymbol{\alpha}_i).$$

Denote $\mathbf{l}_i \sim \text{Dir}^2(\boldsymbol{\alpha}_i)$. Then \mathbf{l}_i has the following density

$$p(\mathbf{l}_i) = p(\mathbf{l}_i^2) |2\mathbf{l}_i| \propto (\mathbf{l}_i^2)^{\boldsymbol{\alpha}_i - 1} |\mathbf{l}_i| = |\mathbf{l}_i|^{2\boldsymbol{\alpha}_i - 1} := \prod_{k=1}^i |l_{ik}|^{2\alpha_{ik} - 1} \quad (7)$$

To induce a prior distribution for the correlation matrix $\mathbf{P} = \mathbf{L}\mathbf{L}^\top$, one can specify priors on row vectors of \mathbf{L} , $\mathbf{l}_i \sim \text{Dir}^2(\boldsymbol{\alpha}_i)$ for $i = 2, \dots, D$. To encourage small correlation, we choose $\boldsymbol{\alpha}_i$ so that the probability density concentrates around the (two) poles of \mathcal{S}_0^{i-1} , e.g. $0 < \alpha_{ik} \ll \alpha_{ii}$ for $k < i$. Figure 2 illustrates the density heat maps of some symmetric squared-Dirichlet distributions $\text{Dir}^2(\alpha \mathbf{1})$ on \mathcal{S}^2 . It is interesting that the squared-Dirichlet distribution induces two important uniform prior distributions over correlation matrices from Barnard et al. (2000) in an effort to provide flexible priors for covariance matrices, as stated in the following theorem.

THEOREM 2 (UNIFORM DISTRIBUTIONS). *Let $\mathbf{P} = \mathbf{L}\mathbf{L}^\top$. Suppose $\mathbf{l}_i \sim \text{Dir}^2(\boldsymbol{\alpha}_i)$, for $i = 2, \dots, D$, are independent, where \mathbf{l}_i is the i -th row of \mathbf{L} . We have the following*

1. If $\boldsymbol{\alpha}_i = (\frac{1}{2}\mathbf{1}_{i-1}^\top, \alpha_{ii})$, $\alpha_{ii} = \frac{(i-2)D-1}{2}$, then \mathbf{P} follows a marginally uniform distribution, that is, $\rho_{ij} \sim \text{Unif}(-1, 1)$, $i \neq j$.
2. If $\boldsymbol{\alpha}_i = (\frac{1}{2}\mathbf{1}_{i-1}^\top, \alpha_{ii})$, $\alpha_{ii} = \frac{D-i}{2} + 1$, then \mathbf{P} follows a jointly uniform distribution, that is, $p(\mathbf{P}) \propto 1$.

Proof. See Section A in the supplementary file. □

Another natural spherical prior can be obtained by constraining a multivariate Gaussian random vector to have unit norm. We denote *unit-vector Gaussian* random variable $\mathbf{l}_i \sim \mathcal{N}_i^{\mathcal{S}}(\boldsymbol{\mu}, \boldsymbol{\Sigma})$

if $\mathbf{l}_i \sim \mathcal{N}_i(\boldsymbol{\mu}, \boldsymbol{\Sigma})$ and $\|\mathbf{l}_i\|_2 = 1$. This is later generalized to a vector Gaussian process constrained to a sphere that serves as a suitable prior for modeling correlation processes. This conditional Gaussian essentially defines the *Fisher-Bingham* distribution (a.k.a. *generalized Kent* distribution, Kent, 1982; Mardia & Jupp, 2009), which reduces to the *von Mises-Fisher* distribution (Fisher, 1953) if $\boldsymbol{\Sigma} = \mathbf{I}$, and the uniform distribution on \mathcal{S}_0^{i-1} if in addition $\boldsymbol{\mu} = \mathbf{0}$. See more details in Section F.1 of the supplementary file.

2.3. Dynamically Modeling the Covariance

We can generalize the proposed framework for modeling covariance/correlation matrices to the dynamic setting by adding subscript t to variables in the model (2) and the model (4), thus called *dynamic covariance* and *dynamic correlation* models respectively. We focus the latter in this section. One can model the components of $\boldsymbol{\sigma}_t$ as independent dynamic processes using, e.g. ARMA, GARCH, or log-Gaussian process. For \mathbf{L}_t , we use vector processes. Since each row of \mathbf{L}_t has to be on a sphere of certain dimension, we require the unit norm constraint for the dynamic process over time. We refer to any multivariate process $\mathbf{l}_i(x)$ satisfying $\|\mathbf{l}_i(x)\| \equiv 1, \forall x \in \mathcal{X}$ as *unit-vector process (uvP)*. A unit-vector process can be obtained by constraining an existing multivariate process, e.g. the *vector Gaussian process (vGP)*, as defined below.

Definition 2 (Vector Gaussian process). A D -dimensional *vector Gaussian process* $\mathbf{Z}(x) := (Z_1(x), \dots, Z_D(x))$, with vector mean function $\boldsymbol{\mu}(x) = (\mu_1(x), \dots, \mu_D(x))$, covariance function \mathcal{C} and (D -dimensional) cross covariance $\mathbf{V}_{D \times D}$, denoted as $\mathbf{Z}(x) \sim \mathcal{GP}_D(\boldsymbol{\mu}, \mathcal{C}, \mathbf{V}_{D \times D})$, is a collection of D -dimensional random vectors, indexed by $x \in \mathcal{X}$, such that for any finite set of indices $\{x_1, \dots, x_N\}$, the random matrix $\tilde{\mathbf{Z}}_{N \times D} := (\mathbf{Z}(x_1), \dots, \mathbf{Z}(x_N))^\top$ has the following matrix normal distribution

$$\tilde{\mathbf{Z}}_{N \times D} \sim \mathcal{MN}_{N \times D}(\mathbf{M}_{N \times D}, \mathbf{K}_{N \times N}, \mathbf{V}_{D \times D})$$

where $\mathbf{M}_{N \times D} := (\mathbf{m}_1, \dots, \mathbf{m}_D)$, and $\mathbf{m}_k = (\mu_k(x_1), \dots, \mu_k(x_N))^\top$, and \mathbf{K} is the kernel matrix with elements $K_{ij} = \mathcal{C}(x_i, x_j)$. \square

Note for each $k = 1, \dots, D$, we have the marginal GP $Z_k(x) \sim \mathcal{GP}(\mu_k, \mathcal{C})$. In the above definition, we require a common kernel \mathcal{C} for all the marginal GPs, whose dependence is characterized by the cross covariance $\mathbf{V}_{D \times D}$. For simplicity, we often consider $\boldsymbol{\mu} \equiv \mathbf{0}$ and $\mathbf{V}_{D \times D} = \mathbf{I}_D$. That is, $Z_k(x) \stackrel{iid}{\sim} \mathcal{GP}(0, \mathcal{C})$ for $k = 1, \dots, D$.

Restricting vGP $\mathbf{Z}(\cdot)$ to sphere yields a *unit-vector Gaussian process (uvGP)* $\mathbf{Z}^*(\cdot) := \mathbf{Z}(\cdot) / \|\mathbf{Z}(\cdot)\|_2 \equiv 1$, denoted as $\mathbf{Z}^*(\cdot) \sim \mathcal{GP}_D^S(\boldsymbol{\mu}, \mathcal{C}, \mathbf{V})$. Note for any fixed $x^* \in \mathcal{X}$, $\mathbf{Z}^*(x^*) \sim \mathcal{N}_D^S(\boldsymbol{\mu}, \mathbf{V})$. Figure 3 shows a realization of vector GP \mathbf{Z}_t , unit-vector GP (forming rows of) \mathbf{L}_t and the induced correlation process \mathbf{P}_t .

In what follows, we focus on multivariate time series; therefore, we use the one dimensional time index $t \in \mathcal{X} = \mathbb{R}^+$. The overall dynamic correlation model can be summarized as follows:

$$\begin{aligned} \mathbf{y}_t &\sim \mathcal{N}(\boldsymbol{\mu}_t, \boldsymbol{\Sigma}_t), & \boldsymbol{\Sigma}_t &= \text{diag}(\boldsymbol{\sigma}_t) \mathbf{L}_t \mathbf{L}_t^\top \text{diag}(\boldsymbol{\sigma}_t) \\ \boldsymbol{\mu}_t &\sim \mathcal{GP}_D(0, \mathcal{C}_\mu, \mathbf{I}), & \mathcal{C}_\mu(t, t') &= \gamma_\mu \exp(-0.5 \|t - t'\|^s / \rho_\mu^s) \\ \log \boldsymbol{\sigma}_t &\sim \mathcal{GP}_D(0, \mathcal{C}_\sigma, \mathbf{I}), & \mathcal{C}_\sigma(t, t') &= \gamma_\sigma \exp(-0.5 \|t - t'\|^s / \rho_\sigma^s) \\ \mathbf{l}_i(t) &\sim \mathcal{GP}_i^S(\mathbf{n}_i, \mathcal{C}_L, \mathbf{I}), & \mathcal{C}_L(t, t') &= \gamma_L \exp(-0.5 \|t - t'\|^s / \rho_L^s) \\ \gamma_* &\sim \Gamma^{-1}(a_*, b_*), & \log \rho_* &\sim \mathcal{N}(m_*, V_*), \quad * = \mu, \sigma, \text{ or } L \end{aligned} \quad (8)$$

where a constant mean function $\mathbf{n}_i = (0, \dots, 0, 1)$ is used in the uvGP prior for $\mathbf{l}_i(t)$. This model (8) captures the spatial dependence in the matrix $\boldsymbol{\Sigma}_t$, which evolves along the time; while the

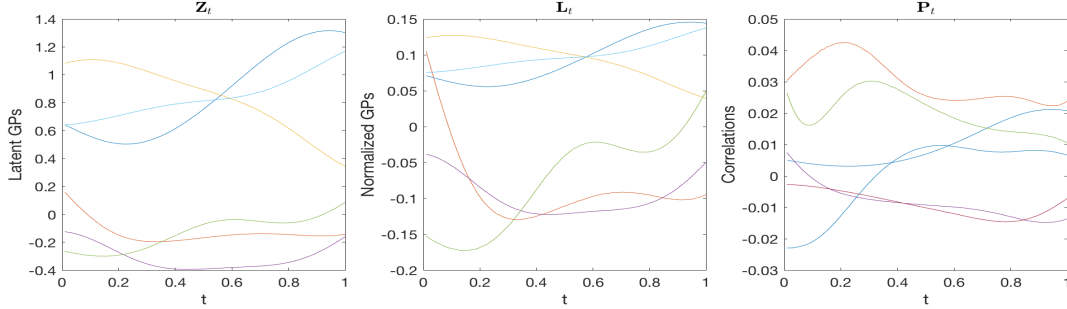


Fig. 3: A realization of vector GP \mathbf{Z}_t (left), unit-vector GP (forming rows of) \mathbf{L}_t (middle) and the induced correlation process \mathbf{P}_t (right).

temporal correlation is characterized by various GPs. The induced covariance process Σ_t is not a generalized Wishart process (Wilson & Ghahramani, 2011), which only models Cholesky factor of covariance using GP. Though with GP, dynamic covariance model may work similarly as the dynamic correlation model (8), yet the latter provides extra flexibility in modeling the evolution of variances and correlations separately. In general such flexibility could be useful in handling constraints for processes, e.g. modeling the dynamic probability for binary time series.

2.4. Posterior Contraction Theorem

We now provide a theorem on the posterior contraction of the dynamic covariance model before we conclude this section. Because the posterior contraction for mean regression using Gaussian process has been thoroughly studied in the literature (van der Vaart & van Zanten, 2008a, 2009, 2011; Yang & Dunson, 2016), we only investigate the covariance regression and set $\mu_t \equiv 0$. We leave the posterior contraction of the dynamic correlation model (8) for future work. Note, the Cholesky decomposition of covariance matrix $\Sigma = \mathbf{L}\mathbf{L}^\top$ is unique if all the diagonal entries of \mathbf{L} are positive. Therefore in the remaining of this section, we identify Cholesky factors up to a column-wise sign, i.e. $\mathbf{L} \sim \mathbf{L} \text{diag}(-\sum_{j \in J} e_j)$ for $J \subset \{1, \dots, D\}$ where e_j is the j -th column of identity matrix \mathbf{I}_D .

In most cases, Gaussian process \mathbf{L}_t can be viewed as a tight Borel measurable map in a Banach space, e.g. a space of continuous functions or L_p space. It is well known that the support of a centered GP is equal to the closure of the *reproducible kernel Hilbert space (RKHS)* \mathbb{H} associated to this process (Lemma 5.1 of van der Vaart & van Zanten, 2008b). Because the posterior distribution necessarily puts all its mass on the support of the prior, the posterior consistency requires the true parameter \mathbf{L}_0 governing the distribution of the data to fall in this support (van der Vaart & van Zanten, 2008a). Following van der Vaart & van Zanten (2008a,b, 2011), we express the rate of the posterior contraction in terms of the *concentration* function

$$\phi_{\mathbf{L}_0}(\varepsilon) = \inf_{h \in \mathbb{H}: \|h - \mathbf{L}_0\| < \varepsilon} \|h\|_{\mathbb{H}}^2 - \log \Pi(\mathbf{L} : \|\mathbf{L}\| < \varepsilon) \quad (9)$$

where $\|\cdot\|$ is the norm of the Banach space where the GP \mathbf{L} takes value, Π is the GP prior and \mathbb{H} is the associated RKHS with norm $\|\cdot\|_{\mathbb{H}}$. Under certain regularity conditions, the posterior contracts with increasing data expressed in n at the rate $\varepsilon_n \rightarrow 0$ satisfying

$$\phi_{\mathbf{L}_0}(\varepsilon_n) \leq n\varepsilon_n^2 \quad (10)$$

Denote $\|\mathbf{L}_t\|_{\infty} := \sup_{t \in \mathcal{X}} \max_{1 \leq i, j \leq D} |l_{ij}(t)|$, and $h(p_1, p_2) := \|\sqrt{p_1} - \sqrt{p_2}\|_2 / \sqrt{2}$ as the Hellinger distance between p_1 and p_2 . Now we state the main theorem of posterior contraction.

THEOREM 3 (POSTERIOR CONTRACTION). *Let $\mathbf{L} - \mathbf{I}$ be a Borel measurable, zero-mean tight Gaussian random element in $\ell^\infty(\mathcal{X})^{D(D+1)/2}$. Suppose that \mathbf{L}_0 is contained in the support of \mathbf{L} and let $\phi_{\mathbf{L}_0}$ be the function in (9) with the uniform norm $\|\cdot\|_\infty$. Then, the posterior distribution relative to the prior $p_{\mathbf{L}}$ satisfies $\mathbb{E}_0 \mathbb{I}_n(p_{\mathbf{L}} : h(p_{\mathbf{L}}, p_0) > M\varepsilon_n | \{t_i, Y_i\}_{i=1}^n) \rightarrow 0$ for any sufficiently large constant M and ε_n given by (10).*

Proof. See Section B in the supplementary file. □

3. POSTERIOR INFERENCE

Now we obtain the posterior probability of mean $\boldsymbol{\mu}_t$, variance $\boldsymbol{\sigma}_t$, Cholesky factor of correlation \mathbf{L}_t , hyper-parameters $\boldsymbol{\gamma} := (\gamma_\mu, \gamma_\sigma, \gamma_L)$ and $\boldsymbol{\rho} := (\rho_\mu, \rho_\sigma, \rho_L)$ in the model (8). Denote the realization of processes $\boldsymbol{\mu}_t, \boldsymbol{\sigma}_t, \mathbf{L}_t$ at discrete time points $\{t_n\}_{n=1}^N$ as $\tilde{\boldsymbol{\mu}}_{N \times D}, \tilde{\boldsymbol{\sigma}}_{N \times D}, \tilde{\mathbf{L}}_{N \times D \times D}$ respectively. Transform the parameters $\tilde{\boldsymbol{\tau}} := \log(\tilde{\boldsymbol{\sigma}})$, $\boldsymbol{\eta} := \log(\boldsymbol{\rho})$ for the convenience of calculation. We use a Metropolis-within-Gibbs algorithm and alternate updating the model parameters $\tilde{\boldsymbol{\mu}}, \tilde{\boldsymbol{\tau}}, \tilde{\mathbf{L}}, \boldsymbol{\gamma}, \boldsymbol{\eta}$. Note, sampling the posterior of $\tilde{\mathbf{L}}$ is the most challenging due to the unit norm constraint of each \mathbf{l}_i . In the following we will use a MCMC algorithm defined on spheres to handle such constraints. Refer to Section C.1 of the supplement for the details of other parameters.

3.1. Spherical HMC

Spherical Hamiltonian Monte Carlo (SphHMC, Lan et al., 2014; Lan & Shahbaba, 2016) is a Hamiltonian Monte Carlo (HMC, Duane et al., 1987; Neal, 2011) algorithm on spheres proposed to handle norm constraints in sampling. It can be used to sample each row of the Cholesky factor of a correlation matrix with unit 2-norm constraint. The following notation \mathbf{q} is instantiated as \mathbf{l}_i .

Assume a probability distribution with density function $f(\mathbf{q})$ is defined on a $(D-1)$ dimensional sphere with radius r , $\mathcal{S}^{D-1}(r)$. Due to the norm constraint, there are $(D-1)$ free parameters $\mathbf{q}_{-D} := (q_1, \dots, q_{D-1})$ that can be viewed as the Cartesian coordinates for the manifold $\mathcal{S}_+^{D-1}(r)$. To induce Hamiltonian dynamics on the sphere, we define the potential energy for position \mathbf{q} as $U(\mathbf{q}) := -\log f(\mathbf{q})$. Endowing the canonical spherical metric $\mathbf{G}(\mathbf{q}_{-D}) = \mathbf{I}_{D-1} + \frac{\mathbf{q}_{-D}\mathbf{q}_{-D}^\top}{q_D^2}$ on the Riemannian manifold $\mathcal{S}^{D-1}(r)$, we introduce the auxiliary velocity vector $\mathbf{v}|\mathbf{q} \sim \mathcal{N}(\mathbf{0}, \mathbf{G}(\mathbf{q})^{-1})$ and define the associated kinetic energy as $K(\mathbf{v}; \mathbf{q}) := -\log f_{\mathcal{N}}(\mathbf{v}|\mathbf{q}) = -\frac{1}{2} \log |\mathbf{G}(\mathbf{q}_{-D})| + \frac{1}{2} \mathbf{v}_{-D}^\top \mathbf{G}(\mathbf{q}_{-D}) \mathbf{v}_{-D}$ (Girolami & Calderhead, 2011). The resulting Lagrangian dynamics can be numerically approximated by a splitting technique which yields the following geometric integrator (Lan et al., 2014; Lan & Shahbaba, 2016):

$$\begin{aligned} \mathbf{v}^- &= \mathbf{v} - \frac{h}{2} \mathcal{P}(\mathbf{q}) \mathbf{g}(\mathbf{q}) \\ \begin{bmatrix} \mathbf{q}' \\ \mathbf{v}^+ \end{bmatrix} &= \begin{bmatrix} r & 0 \\ 0 & \|\mathbf{v}^-\|_2 \end{bmatrix} \begin{bmatrix} \cos(\|\mathbf{v}^-\|_2 r^{-1} h) + \sin(\|\mathbf{v}^-\|_2 r^{-1} h) \\ -\sin(\|\mathbf{v}^-\|_2 r^{-1} h) + \cos(\|\mathbf{v}^-\|_2 r^{-1} h) \end{bmatrix} \begin{bmatrix} r^{-1} & 0 \\ 0 & \|\mathbf{v}^-\|_2^{-1} \end{bmatrix} \begin{bmatrix} \mathbf{q} \\ \mathbf{v}^- \end{bmatrix} \quad (11) \\ \mathbf{v}' &= \mathbf{v}^+ - \frac{h}{2} \mathcal{P}(\mathbf{q}') \mathbf{g}(\mathbf{q}') \end{aligned}$$

where $\mathbf{g}(\mathbf{q}) := \nabla_{\mathbf{q}} \tilde{U}(\mathbf{q})$, $\mathcal{P}(\mathbf{q}) := \mathbf{I}_D - r^{-2} \mathbf{q} \mathbf{q}^\top$. (11) defines a mapping $\mathcal{T}_h : (\mathbf{q}, \mathbf{v}) \mapsto (\mathbf{q}', \mathbf{v}')$. Denote $\|\mathbf{u}\|_{\mathcal{P}(\mathbf{q})}^2 := \mathbf{u}^\top \mathcal{P}(\mathbf{q}) \mathbf{u}$. After applying such integrator T times, a proposal

$(\mathbf{q}_T, \mathbf{v}_T) = \mathcal{T}_h^T(\mathbf{q}_0, \mathbf{v}_0)$ is accepted with the following probability

$$\begin{aligned}
a_{sphHMC} &= 1 \wedge \exp(-\Delta E) \\
\Delta E &= \tilde{U}(\mathbf{q}_T) - \tilde{U}(\mathbf{q}_0) - \frac{h^2}{8} \left[\|\mathbf{g}(\mathbf{q}_T)\|_{\mathcal{P}(\mathbf{q})}^2 - \|\mathbf{g}(\mathbf{q}_0)\|_{\mathcal{P}(\mathbf{q})}^2 \right] \\
&\quad - \frac{h}{2} [\langle \mathbf{v}_0, \mathbf{g}(\mathbf{q}_0) \rangle + \langle \mathbf{v}_T, \mathbf{g}(\mathbf{q}_T) \rangle] - h \sum_{\tau=1}^{T-1} \langle \mathbf{v}_\tau, \mathbf{g}(\mathbf{q}_\tau) \rangle
\end{aligned} \tag{12}$$

We can prove the following limiting result (Beskos et al., 2011).

THEOREM 4. *Let $h \rightarrow 0$ we have the following energy conservation*

$$E(\mathbf{q}(T), \mathbf{v}(T)) - E(\mathbf{q}(0), \mathbf{v}(0)) = \tilde{U}(\mathbf{q}(T)) - \tilde{U}(\mathbf{q}(0)) - \int_0^T \langle \mathbf{v}(t), \mathbf{g}(\mathbf{q}(t)) \rangle dt = 0$$

Proof. See Section D in the supplementary file. \square

Inspired by the ‘No-U-Turn’ sampler (Hoffman & Gelman, 2014), we develop *Adaptive Spherical Hamiltonian Monte Carlo (adp-SphHMC)* (Section D.3 in the supplement) that automatically tunes the number of leapfrog steps and the step size in sampling $\mathbf{l}_i \in \mathcal{S}_0^{i-1}$. To sample \mathbf{L} (or \mathbf{L}_t), we could update each row vector $\mathbf{l}_i \in \mathcal{S}_0^{i-1}$ according to (11) (in parallel), and accept/reject $\text{vech}^\top(\mathbf{L})$ (or $\text{vech}^\top(\mathbf{L}_t)$) simultaneously based on (12) in terms of the sum of total energy of all components. We refer to the resulting algorithm as *Δ -Spherical HMC (Δ -SphHMC)*.

The computational complexity involving GP prior is $\mathcal{O}(N^3)$, and that of the likelihood evaluation is $\mathcal{O}(MD^2)$. MCMC updates of $\tilde{\boldsymbol{\mu}}_{N \times D}$, $\tilde{\boldsymbol{\sigma}}_{N \times D}$, $\tilde{\mathbf{L}}_{N \times D \times D}$ have complexity $\mathcal{O}(ND)$, $\mathcal{O}(ND)$ and $\mathcal{O}(ND^2)$ respectively. To scale up applications to larger dimension D , one could preliminarily classify data into groups, and arrange the corresponding blocks of their covariance/correlation matrix in some ‘band’ along the main diagonal. More specifically, we can assume \mathbf{L}_t is w -band lower triangular matrix for each time t , i.e. $l_{ij} = 0$ for $i < j$ or $i - j \geq w$, then the resulting covariance/correlation matrix will be $(2w - 1)$ -banded. In this way the complexity of likelihood evaluation and updating $\tilde{\mathbf{L}}$ will be reduced to $\mathcal{O}(MwD)$ and $\mathcal{O}(NwD)$ respectively. Therefore the total computational cost would scale linearly with the dimension D . This technique will be explored in Section F.3 of the supplementary file.

4. SIMULATION STUDIES

In this section, we use simulated examples to illustrate the advantage of our structured models for covariance. First, we consider a normal-inverse-Wishart problem, which has been used to verify our structured models (2) (4) in Section 2.1. We investigate flexible priors in Section 2.2 using this example. Then we test our dynamical modeling method in Section 2.3 on a periodic process model. Our model manifests full flexibility compared to a state-of-the-art nonparametric covariance regression model based on latent factor process (Fox & Dunson, 2015).

4.1. Normal-inverse-Wishart Problem

Consider the following example involving inverse-Wishart prior

$$\begin{aligned}
\mathbf{y}_n | \boldsymbol{\Sigma} &\sim \mathcal{N}(\boldsymbol{\mu}_0, \boldsymbol{\Sigma}), \quad n = 1, \dots, N \\
\boldsymbol{\Sigma} &\sim \mathcal{W}_D^{-1}(\boldsymbol{\Psi}, \nu)
\end{aligned} \tag{13}$$

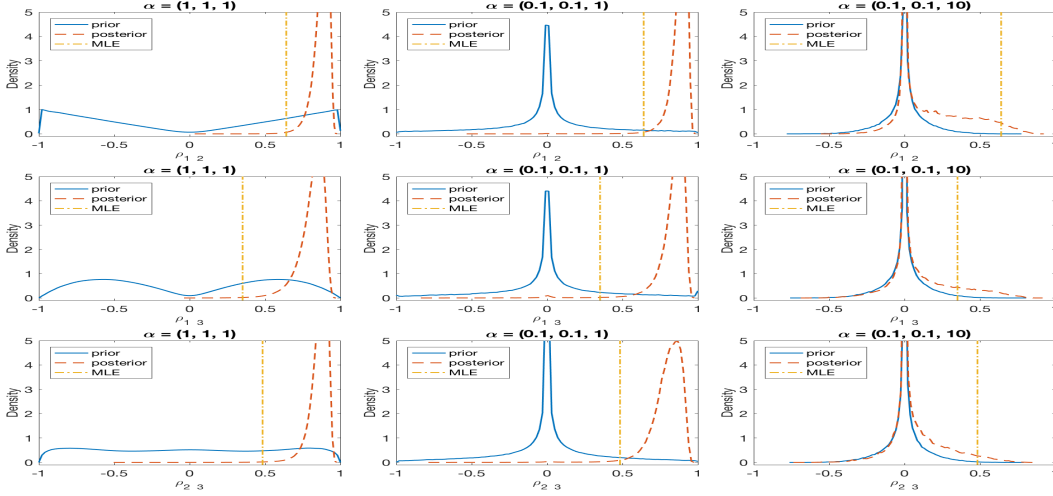


Fig. 4: Marginal posterior, prior (induced from squared-Dirichlet distribution) densities of correlations and MLEs with different settings for concentration parameter α .

It is known that the posterior of $\Sigma|\mathbf{Y}$ is still an inverse-Wishart distribution:

$$\Sigma|\mathbf{Y} \sim \mathcal{W}_D^{-1}(\Psi + (\mathbf{Y} - \boldsymbol{\mu}_0)(\mathbf{Y} - \boldsymbol{\mu}_0)^\top, \nu + N), \quad \mathbf{Y} = [\mathbf{y}_1, \dots, \mathbf{y}_N]^\top \quad (14)$$

We consider dimension $D = 3$ and generate \mathbf{Y} with $\boldsymbol{\mu}_0 = \mathbf{0}$, $\Sigma = \Sigma_0 = \frac{1}{11}(\mathbf{I} + \mathbf{1}\mathbf{1}^\top)$ for $N = 20$ data points so that the prior is not overwhelmed by data.

Now we examine the flexibility of alternative priors in providing prior information for correlation. Specify the following squared-Dirichlet prior (7) for \mathbf{L} in the structured model (4)

$$\begin{aligned} \tau_i = \log(\sigma_i) &\sim \mathcal{N}(0, 0.1^2), \quad i = 1, \dots, D \\ \mathbf{l}_i &\sim \text{Dir}^2(\boldsymbol{\alpha}_i), \quad \boldsymbol{\alpha}_i = (\alpha \mathbf{1}_{i-1}, \alpha_0), \quad i = 2, \dots, D \end{aligned} \quad (15)$$

where we consider three cases i) $\alpha = 1$, $\alpha_0 = 1$; ii) $\alpha = 0.1$, $\alpha_0 = 1$; iii) $\alpha = 0.1$, $\alpha_0 = 10$.

We generate 10^6 prior samples (according to (15)) and posterior samples (by Δ -SphHMC) for \mathbf{L} respectively and convert them to $\mathbf{P} = \mathbf{L}\mathbf{L}^\top$. For each entry ρ_{ij} , the marginal prior/posterior densities (based on samples) with maximal likelihood estimates (MLEs) are plotted in Figure 4. With more and more weight (through α) put around the poles (last component) of each factor sphere, the priors become increasingly dominant that the posteriors (red dash lines) almost fall on priors (blue solid lines) when $\alpha = (0.1, 0.1, 10)$. In this extreme case, the squared-Dirichlet distribution induces priors in favor of trivial (zero) correlations. Similar results regarding the Bingham prior and von Mises-Fisher prior are reported in Section F.1 of the supplementary file.

4.2. Simulated Periodic Processes

In this section, we investigate the performance of our dynamic model (8) on the following periodic process example

$$\begin{aligned} y(t) &\sim \mathcal{N}_D(\boldsymbol{\mu}(t), \Sigma(t)), \quad \Sigma(t) = L(t)L(t)^\top \circ S, \quad t \in [0, 2] \\ \mu_i(t) &= \sin(it\pi/D), \quad L_{ij}(t) = (-1)^i \sin(it\pi/D)(-1)^j \cos(jt\pi/D), \quad j \leq i = 1, \dots, D, \\ S_{ij} &= (|i - j| + 1)^{-1}, \quad i, j = 1, \dots, D \end{aligned} \quad (16)$$

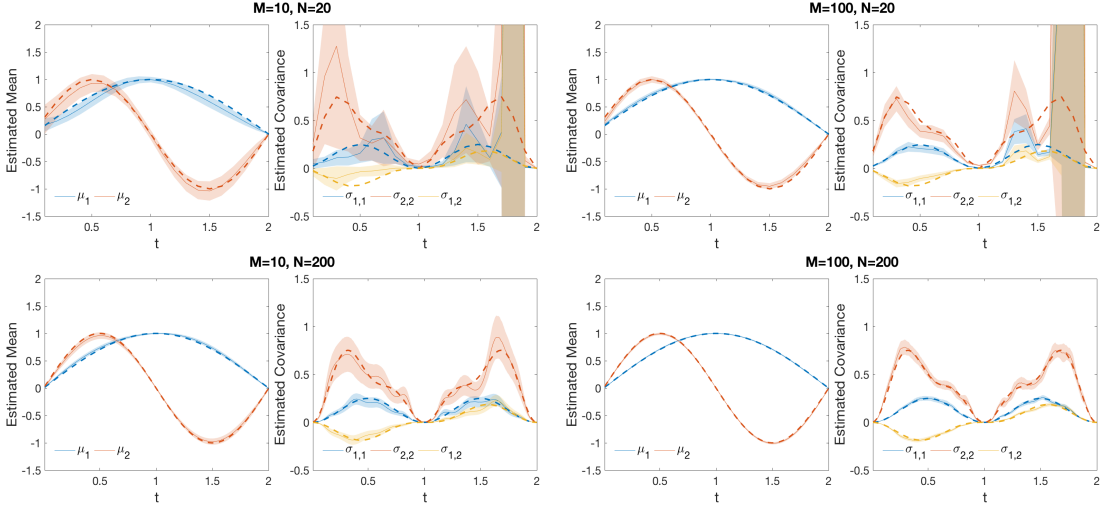


Fig. 5: Estimation of the underlying mean functions μ_t (left in each of 4 subpanels) and covariance functions Σ_t (right in each of 4 subpanels) of 2-dimensional periodic processes. M is the number of trials, and N is the number of discretization points. Dashed lines are true values, solid lines are estimates and shaded regions are 95% credible bands.

Based on the model (16), we generated M trials (process realizations) of data y at N evenly spaced points for t in $[0, 2]$, and therefore the whole data set $\{y(t)\}$ is an $M \times N \times D$ array. We first consider $D = 2$ to investigate the posterior contraction phenomena and the model flexibility; then we consider $D = 100$ over a shorter period $[0, 1]$ to show the scalability using the ‘ w -band’ structure in Section F.3 of the supplementary file.

Posterior Contraction describes the phenomenon that the posterior concentrates on smaller and smaller neighborhood of the true parameter (function) given more and more data (van der Vaart & van Zanten, 2008a). We investigate such phenomena in both mean functions and covariance functions in our model (8) using the following settings *i*) $M = 10, N = 20$; *ii*) $M = 100, N = 20$; *iii*) $M = 10, N = 200$; *iv*) $M = 100, N = 200$.

To fit the data using the model (8), we set $s = 2$, $a = (1, 1, 1)$, $b = (0.1, 10^{-3}, 0.2)$, $m = (0, 0, 0)$ for all settings, $V = (1, 0.5, 1)$ for $N = 20$ and $V = (1, 1, 0.3)$ for $N = 200$. We also add an additional nugget of $10^{-5}I_n$ to all the covariance kernel of GPs to ensure non-degeneracy. We run MCMC for 1.5×10^5 iterations, burn in the first 5×10^4 and subsample 1 for every 10. Based on the resulting 10^4 posterior samples, we estimate the underlying mean functions and covariance functions and plot the estimates in Figure 5.

Note in Figure 5, both M and N have effect on the amount of data information thereafter on the posterior contraction but the contraction rate may depend on them differently. Both mean and covariance functions have narrower credible bands for more discretization points N (comparing $N = 20$ in the first row with $N = 200$ for the second row). On the other hand, both posteriors contract further with more trials M (comparing $M = 10$ in the first column against $M = 100$ for the second column). In general the posterior of mean function contracts to the truth faster than the posterior of covariance function. With $M = 100$ trials and $N = 200$ discretization points, both mean and covariance functions are almost recovered by the model (8).

Full Flexibility can be granted by our method (8) because it models mean, variance and correlation processes separately. This is particularly useful if they behave differently. It contrasts latent

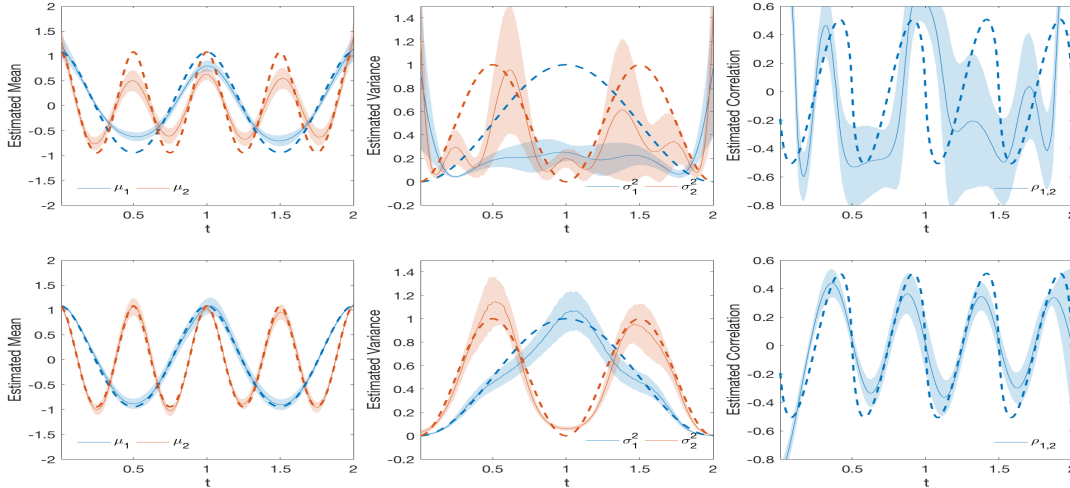


Fig. 6: Estimation of the underlying mean functions μ_t (left column), variance functions σ_t (middle column) and correlation function ρ_t (right column) of 2-dimensional periodic processes, using latent factor process model (upper row) and our flexible model (lower row), based on $M = 10$ trials of data over $N = 200$ evenly spaced points. Dashed lines are true values, solid lines are estimates and shaded regions are 95% credible bands.

factor based models that tie mean and covariance processes together. One of the state-of-the-art models of this type is Bayesian nonparametric covariance regression (Fox & Dunson, 2015):

$$y(x) \sim \mathcal{N}_D(\mu(x), \Sigma(x)), \quad \mu(x) = \Lambda(x)\psi(x), \quad \Sigma(x) = \Lambda(x)\Lambda(x)^\top + \Sigma_0 \quad (17)$$

We tweak the simulated example (16) for $D = 2$ to let mean and correlation processes have higher frequency than variance processes, as shown in the dashed lines in Figure 6. We generate $M = 10$ trials of data over $N = 200$ evenly spaced points. In this case, the true mean processes $\mu(x)$ and true covariance processes $\Sigma(x)$ behave differently but are modeled with a common loading matrix $\Lambda(x)$ in model (17). This imposes difficulty on (17) to have a latent factor process $\psi(x)$ that could properly accommodate the heterogeneity in mean and covariance processes. Figure 6 shows that due to this reason, latent factor based model (17) (upper row) fails to generate satisfactory fit for all of the mean, variance and correlation processes. Our fully flexible model (8) (bottom row), on the contrary, successfully produces more accurate characterization for all of them. See more discussion in Section 6 and more details in Appendices F.2 and F.3.

5. ANALYSIS OF LOCAL FIELD POTENTIAL ACTIVITY

Now we use the proposed model (8) to analyze a local field potential (LFP) activity dataset. The goal of this analysis is to elucidate how memory encoding, retrieval and decision-making arise from functional interactions among brain regions, by modeling how their dynamic connectivity varies during performance of complex memory tasks. Here we focus on LFP activity data recorded from 24 electrodes spanning the dorsal CA1 subregion of the hippocampus as rats performed a sequence memory task (Allen et al., 2014, 2016; Ng et al., 2017; Holbrook et al., 2017). The task involves repeated presentations of a sequence of odors (e.g., ABCDE) at a single port and requires rats to correctly determine whether each odor is presented ‘in sequence’ (InSeq;

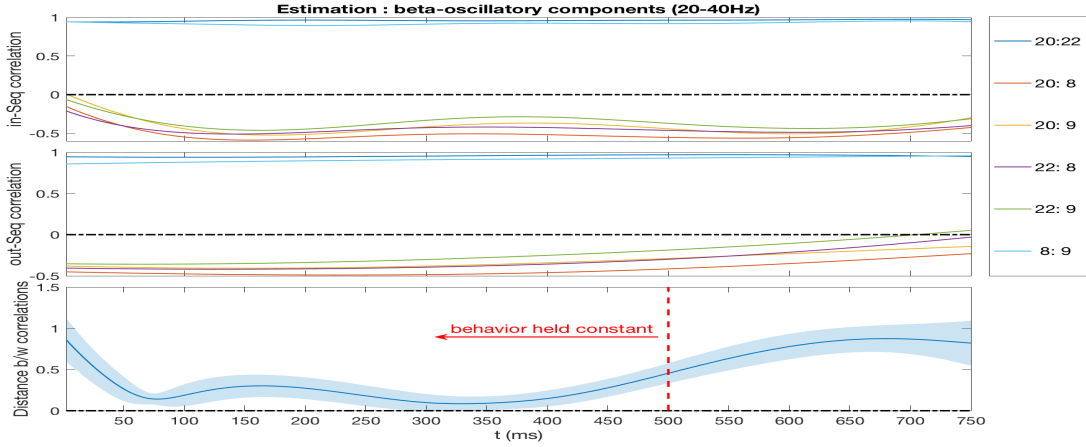


Fig. 7: Estimated correlation processes of LFPs (beta) under InSeq condition (top), OutSeq condition (middle) and the (Frobenius) distance between two correlation matrices (bottom).

e.g., ABCDE; by holding their nosepoke response until the signal at 1.2s) or ‘out of sequence’ (OutSeq; e.g., ABDDE; by withdrawing their nose before the signal). In previous work using the same dataset, Holbrook et al. (2016) used a direct MCMC algorithm to study the spectral density matrix of LFP from 4 selected channels. However, they did not examine how their correlations varied across time and recording site. These limitations are addressed in this paper.

We focus our analyses on the time window from 0ms to 750ms (with 0 corresponding to when the rat’s nose enters the odor port). Critically, this includes a time period during which the behavior of the animal is held constant (0-500ms) so differences in LFP reflect the cognitive processes associated with task performance, and, to serve as a comparison, a time period near 750ms during which the behavioral state of the animal is known to be different (i.e., by 750ms the animal has already withdrawn from the port on the majority of OutSeq trials, but is still in the port on InSeq trials). We also focus our analyses on two sets of adjacent electrodes (electrodes 20 and 22, and electrodes 8 and 9), which allows for comparisons between probes that are near each other (<1 mm; i.e., 20:22 and 8:9) or more distant from each other (>2 mm; i.e., 20:8, 20:9, 22:8, and 22:9). See Section F.4 in the supplement for the figure showing $M = 20$ trials of these LFP signals from $D = 4$ channels under both InSeq and OutSeq conditions. Our main objective is to quantify how correlations among these LFP channels varied across trial types (InSeq vs OutSeq) and over time (within the first 750ms of trials). To do so, we discretize the time window of 0.75 seconds into $N = 300$ equally-spaced small intervals. Under each experiment condition (InSeq or OutSeq), we treat all the signals as a 4 dimensional time series and fit them using our proposed dynamic correlation model (8) in order to discover the evolution of their relationship.

We set $s = 2$, $a = (1, 1, 1)$, $b = (1, 0.1, 0.2)$, $m = (0, 0, 0)$, $V = (1, 1.2, 2)$; and the general results are not very sensitive to the choice of these fine-tuning parameters. We also scale the discretized time points into $(0, 1]$ and add an additional nugget of $10^{-5}I_n$ to the covariance kernel of GPs. We collect 7.5×10^4 samples, burn in the first 2.5×10^4 and subsample 1 for every 10. The resulting 10^4 samples yield estimates of correlation processes as shown in Figure 7 for beta-filtered traces (20-40Hz) but similar patterns were also observed for theta-filtered traces (4-12Hz; see the supplement). The bottom panel of Figure 7 shows the dissimilarity between correlation processes under different conditions measured by the Frobenius norm of their difference.

Our approach revealed many important patterns in the data. First, it showed that electrodes near each other (20:22 and 8:9) displayed remarkably high correlations in their LFP activity on InSeq and OutSeq trials, whereas correlations were considerably lower among more distant electrodes (20:8, 20:9, 22:8, and 22:9). Second, it revealed that the correlations between InSeq and OutSeq matrices evolved during the presentation of individual trials. These results are consistent with other analyses on learning (see, e.g., Fiecas & Ombao, 2016). As expected, InSeq and OutSeq activity was very similar at the beginning of the time window (e.g., before 350ms), which is before the animal has any information about the InSeq or OutSeq status of the presented odor, but maximally different at the end of the time window, which is after it has made its response on OutSeq trials. Most important, however, is the discovery of InSeq vs OutSeq differences before 500ms, which reveal changes in neural activity associated with the complex cognitive process of identifying if events occurred in their expected order. These findings highlight the sensitivity of our novel approach, as such differences have not been detected with traditional analyses.

6. CONCLUSION

In this paper, we propose a novel Bayesian framework that grants full flexibility in modeling covariance and correlation matrices. It extends the separation strategy proposed by Barnard et al. (2000) and uses the Cholesky decomposition to maintain the positive definiteness of the correlation matrix. By defining distributions on spheres, a large class of flexible priors can be induced for covariance matrix that go beyond the commonly used but restrictive inverse-Wishart distribution. Adaptive Δ -Spherical HMC is introduced to handle the intractability of the resulting posterior. Furthermore, we extend this structured scheme to dynamical models to capture complex dependence among multiple stochastic processes, and demonstrate the effectiveness and efficiency in Bayesian modeling covariance and correlation matrices using a normal-inverse-Wishart problem, a simulated periodic process, and an analysis of LFP data. In addition, we provide both theoretic characterization and empirical investigation of posterior contraction for dynamically covariance modeling, which to our best knowledge, is a first attempt.

In future work, we will explore the low-rank structure of covariance and correlation matrices to further scale our method to problems of greater dimensionality. For example, we can adopt the similar factor analysis as in Fox & Dunson (2015), and assume $\text{vech}^\top(\mathbf{L}_t) \in (\mathcal{S}^k)^D$ for some $k \ll D$.

While our research has generated interesting new findings regarding brain signals during memory tasks, one limitation of our current analysis on LFP data is that it is conducted on a single rat. The proposed model can be generalized to account for variation among rats. In the future, we will apply this sensitive approach to other datasets, including simultaneous LFP recordings from multiple brain regions in rats as well as BOLD fMRI data collected from human subjects performing the same task.

ACKNOWLEDGEMENTS

SL was supported by ONR N00014-17-1-2079. AH is supported by NIH grant T32 AG000096. GAE is supported by NIDCD T32 DC010775. NJF is supported by NSF awards IOS-1150292 and BCS-1439267 and Whitehall Foundation award 2010-05-84. HO is supported by NSF DMS 1509023 and NSF SES 1461534. BS is supported by NSF DMS 1622490 and NIH R01 AI107034. We thank Yulong Lu at Duke for discussions on posterior contraction of covariance regression with Gaussian processes.

SUPPLEMENTARY MATERIAL

A. CONNECTION TO KNOWN PRIORS

The following lemma is essential in proving that our proposed methods (2) (4) generalize existing methods in specifying priors, including the inverse-Wishart distribution, and two uniform distributions (Barnard et al., 2000) as well.

Lemma A.1. Let $\Sigma = \mathbf{U}\mathbf{U}^\top$ be the reversed Cholesky decomposition of Σ . The Jacobian of the transformation $\Sigma \mapsto \mathbf{U}$ is

$$\left| \frac{d_h \Sigma}{d_h \mathbf{U}^\top} \right| := \left| \frac{\partial \text{vech} \Sigma}{\partial \text{vech} \mathbf{U}^\top} \right| = 2^D \prod_{i=1}^D |u_{ii}|^i$$

Let $\mathbf{P} = \mathbf{L}\mathbf{L}^\top$ be the Cholesky decomposition of \mathbf{P} . The Jacobian of the transformation $\mathbf{L} \mapsto \mathbf{P}$ is

$$\left| \frac{d_h \mathbf{L}}{d_h \mathbf{P}} \right| := \left| \frac{\partial \text{vech} \mathbf{L}}{\partial \text{vech} \mathbf{P}} \right| = 2^{-D} \prod_{i=1}^D |l_{ii}|^{i-(D+1)}$$

Proof. Note we have

$$d\Sigma = d\mathbf{U}\mathbf{U}^\top + \mathbf{U}d\mathbf{U}^\top$$

Taking vec on both sides and applying its property

$$d\text{vec} \Sigma = (\mathbf{U} \otimes \mathbf{I})d\text{vec} \mathbf{U} + (\mathbf{I} \otimes \mathbf{U})d\text{vec} \mathbf{U}^\top$$

Applying the elimination \mathbf{L}_D on both sides

$$\begin{aligned} d\text{vech} \Sigma &= \mathbf{L}_D [(\mathbf{U} \otimes \mathbf{I})\mathbf{K}_D d\text{vec} \mathbf{U}^\top + (\mathbf{I} \otimes \mathbf{U})d\text{vec} \mathbf{U}^\top] = \mathbf{L}_D (\mathbf{K}_D + \mathbf{I})(\mathbf{I} \otimes \mathbf{U})d\text{vec} \mathbf{U}^\top \\ &= 2\mathbf{L}_D \mathbf{N}_D (\mathbf{I} \otimes \mathbf{U})\mathbf{L}_D^\top d\text{vech} \mathbf{U}^\top = 2\mathbf{L}_D \mathbf{N}_D \mathbf{L}_D^\top \mathbf{D}_D^\top (\mathbf{I} \otimes \mathbf{U})\mathbf{L}_D^\top d\text{vech} \mathbf{U}^\top \end{aligned}$$

where \mathbf{K}_D is the *commutation matrix* such that $\mathbf{K}_D \text{vec} \mathbf{A} = \text{vec} \mathbf{A}^\top$ for matrix $\mathbf{A}_{D \times D}$, $\mathbf{N}_D := (\mathbf{K}_D + \mathbf{I})/2$, and \mathbf{D}_D is the *duplication matrix* which is regarded as the inverse of the elimination matrix \mathbf{L}_D . The last equation is by $\mathbf{D}_D \mathbf{L}_D \mathbf{N}_D = \mathbf{N}_D = \mathbf{N}_D^\top$ (Lemma 2.1 and Lemma 3.5 in Magnus & Neudecker, 1980). Thus according to (Lemma 3.4 and Lemma 4.1 in Magnus & Neudecker, 1980) we have

$$\begin{aligned} \left| \frac{d_h \Sigma}{d_h \mathbf{U}^\top} \right| &= \left| \frac{\partial \text{vech} \Sigma}{\partial \text{vech} \mathbf{U}^\top} \right| = |2\mathbf{L}_D \mathbf{N}_D \mathbf{L}_D^\top \mathbf{D}_D^\top (\mathbf{I} \otimes \mathbf{U})\mathbf{L}_D^\top| \\ &= 2^{D(D+1)/2} |\mathbf{L}_D \mathbf{N}_D \mathbf{L}_D^\top| |\mathbf{L}_D (\mathbf{I} \otimes \mathbf{U}^\top) \mathbf{D}_D| = 2^D \prod_{i=1}^D |u_{ii}^i| \end{aligned}$$

By similar argument, we have

$$\begin{aligned} \left| \frac{d_h \mathbf{P}}{d_h \mathbf{L}} \right| &= \left| \frac{\partial \text{vech} \mathbf{P}}{\partial \text{vech} \mathbf{L}} \right| = |2\mathbf{L}_D \mathbf{N}_D \mathbf{L}_D^\top \mathbf{D}_D^\top (\mathbf{L} \otimes \mathbf{I})\mathbf{L}_D^\top| \\ &= 2^{D(D+1)/2} |\mathbf{L}_D \mathbf{N}_D \mathbf{L}_D^\top| |\mathbf{L}_D (\mathbf{L}^\top \otimes \mathbf{I}) \mathbf{D}_D| = 2^D \prod_{i=1}^D |l_{ii}|^{D+1-i}. \end{aligned}$$

Thus it completes the proof. □

Proof of Theorem 1. We know that the density of $\Sigma \sim \mathcal{W}_D^{-1}(\Psi, \nu)$ is

$$p_{\mathcal{W}^{-1}}(\Sigma; \Psi, \nu) = \frac{|\Psi|^{\nu/2}}{2^{D\nu/2} \Gamma_D(\nu/2)} |\Sigma|^{-(\nu+D+1)/2} \exp\left(-\frac{1}{2} \text{tr}(\Psi \Sigma^{-1})\right)$$

By Lemma A.1 we have

$$\begin{aligned} p(\mathbf{U}) &= p(\boldsymbol{\Sigma}) \left| \frac{d_h \boldsymbol{\Sigma}}{d_h \mathbf{U}^\top} \right| = 2^D p_{\mathcal{W}^{-1}}(\mathbf{U} \mathbf{U}^\top; \boldsymbol{\Psi}, \nu) \prod_{i=1}^D |u_{ii}^i| \\ &= \frac{|\boldsymbol{\Psi}|^{\nu/2}}{2^{D(\nu-2)/2} \Gamma_D(\nu/2)} |\mathbf{U}|^{-(\nu+D+1)} \prod_{i=1}^D u_{ii}^i \exp\left(-\frac{1}{2} \text{tr}(\boldsymbol{\Psi} \mathbf{U}^{-\top} \mathbf{U}^{-1})\right). \end{aligned}$$

Then the proof is completed. \square

Proof of Theorem 2. To prove the first result, we use Lemma A.1

$$p(\mathbf{P}) = p(\mathbf{L}) \left| \frac{d_h \mathbf{L}}{d_h \mathbf{P}} \right| \propto \prod_{i=2}^D |l_i|^{2\alpha_i-1} \prod_{i=1}^D |l_{ii}|^{i-(D+1)} = \prod_{i=1}^D |l_{ii}|^{(i-3)(D+1)}$$

On the other hand, from Equation (8) in Barnard et al. (2000), we have the density of marginally uniform distribution:

$$p(\mathbf{P}) \propto |\mathbf{P}|^{\frac{D(D-1)}{2}-1} \left(\prod_i \mathbf{P}_{ii} \right)^{-\frac{D+1}{2}} = \left(\prod_{j=1}^D l_{jj}^2 \right)^{\frac{D(D-1)}{2}-1} \left(\prod_{j=1}^D \prod_{i=1}^j l_{ii}^2 \right)^{-\frac{D+1}{2}} = \prod_{j=1}^D |l_{jj}|^{(j-3)(D+1)}$$

where \mathbf{P}_{ii} is the i -th principal minor of \mathbf{P} . Similarly by Lemma A.1 we can prove the second result

$$p(\mathbf{P}) = p(\mathbf{L}) \left| \frac{d_h \mathbf{L}}{d_h \mathbf{P}} \right| \propto \prod_{i=2}^D |l_i|^{2\alpha_i-1} \prod_{i=1}^D |l_{ii}|^{i-(D+1)} \propto 1.$$

Therefore we have finished the proof. \square

B. POSTERIOR CONTRACTION

For the Gaussian likelihood models $p_i \sim \mathcal{N}(\boldsymbol{\mu}_i(t), \boldsymbol{\Sigma}_i(t))$ for $i = 0, 1$, we first bound the Hellinger distance, Kullback-Leibler distance and variance distance $V(p_0, p_1) = \mathbb{E}_0(\log(p_0/p_1))^2$ with the uniform norm in the following lemma. Notation \lesssim means ‘‘smaller than or equal to a universal constant times’’.

Lemma B.1. For any bounded measurable functions $\boldsymbol{\Sigma}_i : \mathcal{X} \rightarrow \mathbb{R}^{D^2}$ with Cholesky decompositions $\boldsymbol{\Sigma}_i = \mathbf{L}_i \mathbf{L}_i^\top$, assume $\inf_{t \in \mathcal{X}} \max_{1 \leq j \leq D} |l_{i,jj}(t)| \geq c_0 > 0$, $i = 0, 1$. Then we have

- $h(p_0, p_1) \lesssim \|\mathbf{L}_0 - \mathbf{L}_1\|_\infty^{\frac{1}{2}}$
- $K(p_0, p_1) \lesssim \|\mathbf{L}_0 - \mathbf{L}_1\|_\infty$
- $V(p_0, p_1) \lesssim \|\mathbf{L}_0 - \mathbf{L}_1\|_\infty^2$

\square

Proof. First we calculate

$$\begin{aligned} \log p_0 - \log p_1 &= \frac{1}{2} \left\{ \log \frac{|\boldsymbol{\Sigma}_1|}{|\boldsymbol{\Sigma}_0|} + (\mathbf{y} - \boldsymbol{\mu}_*)^\top \boldsymbol{\Sigma}_*^{-1} (\mathbf{y} - \boldsymbol{\mu}_*) + ** \right\} \\ \boldsymbol{\Sigma}_*^{-1} &= \boldsymbol{\Sigma}_1^{-1} - \boldsymbol{\Sigma}_0^{-1}, \quad \boldsymbol{\mu}_* = \boldsymbol{\Sigma}_* (\boldsymbol{\Sigma}_1^{-1} \boldsymbol{\mu}_1 - \boldsymbol{\Sigma}_0^{-1} \boldsymbol{\mu}_0) \\ ** &= -(\boldsymbol{\mu}_1 - \boldsymbol{\mu}_0)^\top \boldsymbol{\Sigma}_1^{-1} \boldsymbol{\Sigma}_* \boldsymbol{\Sigma}_0^{-1} (\boldsymbol{\mu}_1 - \boldsymbol{\mu}_0) \end{aligned} \tag{B.1}$$

Taking expectation of (B.1) with respect to p_0 yields the following Kullback-Leibler divergence

$$K(p_0, p_1) = \frac{1}{2} \left\{ \text{tr}(\boldsymbol{\Sigma}_1^{-1} \boldsymbol{\Sigma}_0) + (\boldsymbol{\mu}_1 - \boldsymbol{\mu}_0)^\top \boldsymbol{\Sigma}_1^{-1} (\boldsymbol{\mu}_1 - \boldsymbol{\mu}_0) - D + \log \frac{|\boldsymbol{\Sigma}_1|}{|\boldsymbol{\Sigma}_0|} \right\}$$

Consider $\boldsymbol{\mu}_i \equiv 0$. By the non-negativity of K-L divergence we have for general $\boldsymbol{\Sigma}_i > 0$,

$$\log \frac{|\boldsymbol{\Sigma}_0|}{|\boldsymbol{\Sigma}_1|} \leq \text{tr}(\boldsymbol{\Sigma}_1^{-1} \boldsymbol{\Sigma}_0 - \mathbf{I}) \quad (\text{B.2})$$

Therefore we can bound K-L divergence

$$K(p_0, p_1) \leq \frac{1}{2} \{ \text{tr}(\boldsymbol{\Sigma}_1^{-1} \boldsymbol{\Sigma}_0 - \mathbf{I}) + \text{tr}(\boldsymbol{\Sigma}_0^{-1} \boldsymbol{\Sigma}_1 - \mathbf{I}) \} \leq C(D, c_0) \|\boldsymbol{\Sigma}_0 - \boldsymbol{\Sigma}_1\|_\infty \lesssim \|\mathbf{L}_0 - \mathbf{L}_1\|_\infty$$

where we use

$$\begin{aligned} \text{tr}(\boldsymbol{\Sigma}_1^{-1} \boldsymbol{\Sigma}_0 - \mathbf{I}) &= \text{tr}(\boldsymbol{\Sigma}_1^{-1} (\boldsymbol{\Sigma}_0 - \boldsymbol{\Sigma}_1)) \leq \|\boldsymbol{\Sigma}_1^{-1}\|_F \|\boldsymbol{\Sigma}_0 - \boldsymbol{\Sigma}_1\|_F \\ &\leq D^{3/2} \|\boldsymbol{\Sigma}_1^{-1}\|_2 \|\boldsymbol{\Sigma}_0 - \boldsymbol{\Sigma}_1\|_\infty \leq D^{3/2} c_0^2 (\|\mathbf{L}_0\|_\infty + \|\mathbf{L}_1\|_\infty) \|\mathbf{L}_0 - \mathbf{L}_1\|_\infty \end{aligned} \quad (\text{B.3})$$

Now take expectation of squared (B.1) with respect with p_0 to get the following variance distance

$$V(p_0, p_1) = \frac{1}{2} \text{tr}((\boldsymbol{\Sigma}_1^{-1} \boldsymbol{\Sigma}_0 - \mathbf{I})^2) + (\boldsymbol{\mu}_1 - \boldsymbol{\mu}_0)^\top \boldsymbol{\Sigma}_1^{-1} \boldsymbol{\Sigma}_0 \boldsymbol{\Sigma}_1^{-1} (\boldsymbol{\mu}_1 - \boldsymbol{\mu}_0) + K^2(p_0, p_1)$$

Consider $\boldsymbol{\mu}_i \equiv 0$ and we can bound the variance distance by similar argument as (B.3)

$$V(p_0, p_1) \leq \frac{1}{2} \|\boldsymbol{\Sigma}_1^{-1} (\boldsymbol{\Sigma}_0 - \boldsymbol{\Sigma}_1)\|_F^2 + K^2(p_0, p_1) \leq C \|\boldsymbol{\Sigma}_1^{-1}\|_F^2 \|\boldsymbol{\Sigma}_0 - \boldsymbol{\Sigma}_1\|_F^2 + K^2(p_0, p_1) \lesssim \|\mathbf{L}_0 - \mathbf{L}_1\|_\infty^2$$

where we use the fact $\|\mathbf{AB}\|_F \leq \|\mathbf{A}\|_F \|\mathbf{B}\|_F$.

Lastly, the squared Hellinger distance for multivariate Gaussians can be calculated

$$h^2(p_0, p_1) = 1 - \frac{|\boldsymbol{\Sigma}_0 \boldsymbol{\Sigma}_1|^{1/4}}{\left| \frac{\boldsymbol{\Sigma}_0 + \boldsymbol{\Sigma}_1}{2} \right|^{1/2}} \exp \left\{ (\boldsymbol{\mu}_0 - \boldsymbol{\mu}_1)^\top \left(\frac{\boldsymbol{\Sigma}_0 + \boldsymbol{\Sigma}_1}{2} \right)^{-1} (\boldsymbol{\mu}_0 - \boldsymbol{\mu}_1) \right\}$$

Consider $\boldsymbol{\mu}_i \equiv 0$. Notice that $1 - x \leq -\log x$, and by (B.2) we can bound the squared Hellinger distance using similar argument in (B.3)

$$\begin{aligned} h^2(p_0, p_1) &\leq \log \frac{\left| \frac{\boldsymbol{\Sigma}_0 + \boldsymbol{\Sigma}_1}{2} \right|^{1/2}}{|\boldsymbol{\Sigma}_0 \boldsymbol{\Sigma}_1|^{1/4}} \leq \frac{1}{2} \text{tr}(\mathbf{L}_0^{-\top} \mathbf{L}_1^{-1} (\boldsymbol{\Sigma}_0 + \boldsymbol{\Sigma}_1)/2 - \mathbf{I}) \\ &= \frac{1}{4} \{ \text{tr}(\mathbf{L}_1^{-1} \mathbf{L}_0 - \mathbf{I}) + \text{tr}(\mathbf{L}_0^{-\top} \mathbf{L}_1^\top - \mathbf{I}) \} \leq \frac{D^{3/2} c_0}{2} \|\mathbf{L}_0 - \mathbf{L}_1\|_\infty \end{aligned}$$

Therefore we complete the proof. \square

Define the following *coordinate concentration* function as in (9)

$$\phi_{l_0, ij}(\varepsilon) = \inf_{h_{ij} \in \mathbb{H}_{ij}: \|h_{ij} - l_{0, ij}\|_{ij} < \varepsilon} \|h\|_{\mathbb{H}_{ij}}^2 - \log \Pi(l_{ij} : \|l_{ij}\|_{ij} < \varepsilon) \quad (\text{B.4})$$

It is easy to see that $\phi_{l_0, ij}(\varepsilon) \leq \phi_{\mathbf{L}_0}(\varepsilon)$ for $\forall 1 \leq j \leq i \leq D$. Let $\|\cdot\| := \max_{i,j} \|\cdot\|_{ij}$. For $\varepsilon > 0$, let $N(\varepsilon, B, d)$ denote the minimum number of balls of radius ε that a cover B in a metric space with metric d , which is named ε -covering number for B . Now we prove a theorem similar as Theorem 2.1 of van der Vaart & van Zanten (2008a).

THEOREM B.1. *Let \mathbf{L} be a Borel measurable, zero-mean Gaussian random element in a separable Banach space $(\mathbb{B}^{D(D+1)/2}, \|\cdot\|)$ with RKHS $(\mathbb{H}^{D(D+1)/2}, \|\cdot\|_{\mathbb{H}})$ and let \mathbf{L}_0 be contained in the closure of $\mathbb{H}^{D(D+1)/2}$ in $\mathbb{B}^{D(D+1)/2}$. For any numbers $\varepsilon_n > 0$ satisfying (10) for $\phi_{\mathbf{L}_0}$ given by (9), and any $C > 1$ with $e^{-Cn\varepsilon_n^2} < 1/2$, there exists a measurable set $B_n \subset \mathbb{B}^{D(D+1)/2}$ such that*

$$\log N(3\varepsilon_n, B_n, \|\cdot\|) \leq 6Cn\varepsilon_n^2, \quad (\text{B.5a})$$

$$\Pi(\mathbf{L} \notin B_n) \leq e^{-Cn\varepsilon_n^2}, \quad (\text{B.5b})$$

$$\Pi(\|\mathbf{L} - \mathbf{L}_0\| < 2\varepsilon_n) \geq e^{-n\varepsilon_n^2}. \quad (\text{B.5c})$$

Proof. Equation (10) implies $\phi_{l_{0,ij}}(\varepsilon_n) \leq n\varepsilon_n^2$, for $1 \leq j \leq i \leq D$. We apply Theorem 2.1 of van der Vaart & van Zanten (2008a) to each coordinate l_{ij} to get $B_{n,ij} \subset \mathbb{B}$ satisfying conditions (B.5). Set $B_n = \prod_{i,j} B_{n,ij} := \{\mathbf{L} : l_{ij} \in B_{n,ij}\}$, and $N(3\varepsilon, B_n, \|\cdot\|) = \max_{i,j} N_{ij}(3\varepsilon, B_{n,ij}, \|\cdot\|_{ij})$. Then we have (B.5a). Note $\Pi(\mathbf{L} \notin B_n) \leq e^{-Cn\varepsilon_n^2} \leq \sum_{i,j} \Pi(l_{ij} \notin B_{n,ij}) \leq \frac{D(D+1)}{2} e^{-C'n\varepsilon_n^2}$ thus we have (B.5b). Finally, $\Pi(\|\mathbf{L} - \mathbf{L}_0\| \geq 2\varepsilon_n) \leq \Pi(\|l_{\arg \max} - l_{0, \arg \max}\| \geq 2\varepsilon_n) \leq 1 - e^{-n\varepsilon_n^2}$ therefore we have (B.5c) by inverting the inequality. \square

Now we are ready to prove the theorem of posterior concentration.

Proof of Theorem 3. The proof follows in the same vein of Theorem 3.1 of van der Vaart & van Zanten (2008a) to combine Theorem 2.1 of Ghosal et al. (2000) and Theorem B.1. First apply Theorem B.1 for $\mathbf{L} - \mathbf{I}$ to obtain B_n for \mathbf{L} satisfying conditions (B.5).

We choose the set \mathcal{P}_n of Ghosal et al. (2000) equal to $\{p_{\mathbf{L}} : \mathbf{L} \in B_n\}$, with $B_n \subset \ell^\infty(\mathcal{X})^{D(D+1)/2}$ being the measurable set as in Theorem B.1. With Lemma B.1 the $4\varepsilon_n$ -entropy of \mathcal{P}_n relative to Hellinger distance is bounded above by the $3\varepsilon_n^2$ -entropy of the set B_n relative to the uniform distance, which is bounded by $6Cn\varepsilon_n^2$ by Theorem B.1. This verifies (2.2) of Ghosal et al. (2000). The prior probability $\Pi(\mathcal{P}_n^c)$ outside the set \mathcal{P}_n in (2.3) of Ghosal et al. (2000) is bounded by the probability of the event $\{\mathbf{L} \notin B_n\}$, which is bounded by $e^{-Cn\varepsilon_n^2}$, by Theorem B.1. Finally, by the second and third inequalities of Lemma B.1, the prior probability in (2.4) of Ghosal et al. (2000), is bounded below by the probability of the event $\{\|\mathbf{L} - \mathbf{L}_0\| < 2\varepsilon_n\}$, which is bounded below by $e^{-n\varepsilon_n^2}$, by Theorem B.1. \square

Remark B.1. In principle, the smoothness of GP should match the regularity of the true parameter to achieve the optimal rate of contraction (van der Vaart & van Zanten, 2008a, 2011). One can scale GP, e.g. using an inverse-Gamma bandwidth, to get optimal contraction rate for every regularity level so that the resulting estimator is rate adaptive (van der Vaart & van Zanten, 2009, 2011). One can refer to Section 3.2 of (van der Vaart & van Zanten, 2011) for posterior contraction rates using squared exponential kernel for GP. We leave further investigation on contraction rates in the setting of covariance regression to future work. \square

Remark B.2. Here the GP prior \mathbf{L} defines a (mostly finite) probability measure on the space of bounded functions. The true parameter function \mathbf{L}_0 is required to be contained in the support of the prior, the RKHS of \mathbf{L} . The contraction rate depends on the position of \mathbf{L}_0 relative to the RKHS and the small-ball probability $\Pi(\|\mathbf{L}\| < \varepsilon)$. \square

C. POSTERIOR INFERENCE

C.1. Metropolis-within-Gibbs

Denote $\tilde{\mathbf{Y}}_{M \times N \times D} := \{\mathbf{Y}_1, \dots, \mathbf{Y}_M\}$ for M trials, $(\mathbf{Y}_m)_{N \times D} := [\mathbf{y}_{m1}, \dots, \mathbf{y}_{mN}]^\top$ and $\mathbf{y}_{mn}^* := (\mathbf{y}_{mn} - \boldsymbol{\mu}_n) \circ e^{-\boldsymbol{\tau}_n}$ where \circ is the Hadamard product (a.k.a. Schur product), i.e. the entry-wise product. Let $\mathbf{K}_*(\gamma_*, \eta_*) = \gamma_* \mathbf{K}_{0*}(\eta_*)$ and $\tilde{\mathbf{I}}_i^* := \tilde{\mathbf{I}}_i - \mathbf{1}_N \otimes \mathbf{n}_i^\top$. We use a Metropolis-within-Gibbs algorithm and alternate updating the model parameters $\tilde{\boldsymbol{\mu}}, \tilde{\boldsymbol{\tau}}, \tilde{\mathbf{L}}, \boldsymbol{\gamma}, \boldsymbol{\eta}$. We now list the parameters and their respective updates one by one.

($\boldsymbol{\gamma}$). Note the prior for $\boldsymbol{\gamma}$ is conditionally conjugate given $*$ = μ, τ , or L ,

$$\boldsymbol{\gamma}_* | \tilde{*, \eta_*} \sim \Gamma^{-1}(a'_*, b'_*), \quad a'_* = a_* + \frac{ND}{2} ((D+1)/2 - D^{-1})^{[*=L]}, \quad b'_* = b_* + \frac{1}{2} \text{tr}(\tilde{*}^\top \mathbf{K}_{0*}(\eta_*)^{-1} \tilde{*})$$

where [condition] is 1 with the condition satisfied and 0 otherwise.

($\boldsymbol{\eta}$). Given $*$ = μ, τ , or L , we could sample η_* using the slice sampler (Neal, 2003), which only requires log-posterior density and works well for scalar parameters,

$$\log p(\eta_* | \tilde{*, \boldsymbol{\gamma}_*}) = -\frac{D(\frac{D+1}{2} - D^{-1})^{[*=L]}}{2} \log |\mathbf{K}_{0*}(\eta_*)| - \frac{1}{2} \text{tr}(\tilde{*}^\top \mathbf{K}_{0*}(\eta_*)^{-1} \tilde{*}) / \boldsymbol{\gamma}_* - \frac{1}{2} (\eta_* - m_*)^2 / V_*$$

($\tilde{\boldsymbol{\mu}}$). By the definition of vGP, we have $\tilde{\boldsymbol{\mu}}|\gamma_\mu, \eta_\mu \sim \mathcal{MN}_{N \times D}(\mathbf{0}, \mathbf{K}_\mu, \mathbf{I}_D)$; therefore, $\text{vec}(\tilde{\boldsymbol{\mu}})|\gamma_\mu, \eta_\mu \sim \mathcal{N}_{ND}(\mathbf{0}, \mathbf{I}_D \otimes \mathbf{K}_\mu)$. On the other hand, one can write

$$\begin{aligned} \sum_{m=1}^M \sum_{n=1}^N \mathbf{y}_{mn}^* \mathbf{P}_n^{-1} \mathbf{y}_{mn}^* &= \sum_{m=1}^M \text{vec}((\mathbf{Y}_m - \tilde{\boldsymbol{\mu}})^\top)^\top \text{diag}(\{\tilde{\boldsymbol{\Sigma}}_n^{-1}\}) \text{vec}((\mathbf{Y}_m - \tilde{\boldsymbol{\mu}})^\top) \\ &= \sum_{m=1}^M (\text{vec}(\mathbf{Y}_m) - \text{vec}(\tilde{\boldsymbol{\mu}}))^\top \tilde{\boldsymbol{\Sigma}}_K^{-1} (\text{vec}(\mathbf{Y}_m) - \text{vec}(\tilde{\boldsymbol{\mu}})) \end{aligned}$$

where $\tilde{\boldsymbol{\Sigma}}_K^{-1} := K_{(D,N)} \text{diag}(\{\tilde{\boldsymbol{\Sigma}}_n\})^{-1} K_{(N,D)}$, and $K_{(N,D)}$ is the *commutation matrix* of size $ND \times ND$ such that for any $N \times D$ matrix \mathbf{A} , $K_{(N,D)} \text{vec}(\mathbf{A}) = \text{vec}(\mathbf{A}^\top)$ (Tracy & Dwyer, 1969; Magnus & Neudecker, 1979). Therefore, the prior on $\text{vec}(\tilde{\boldsymbol{\mu}})$ is conditionally conjugate, and we have

$$\text{vec}(\tilde{\boldsymbol{\mu}})|\tilde{\mathbf{Y}}, \tilde{\boldsymbol{\Sigma}}, \gamma_\mu, \eta_\mu \sim \mathcal{N}_{ND}(\boldsymbol{\mu}', \boldsymbol{\Sigma}'), \quad \boldsymbol{\mu}' = \boldsymbol{\Sigma}' \tilde{\boldsymbol{\Sigma}}_K^{-1} \sum_{m=1}^M \text{vec}(\mathbf{Y}_m), \quad \boldsymbol{\Sigma}' = \left(\mathbf{I}_D \otimes \mathbf{K}_\mu^{-1} + M \tilde{\boldsymbol{\Sigma}}_K^{-1} \right)^{-1}$$

($\tilde{\boldsymbol{\tau}}$). Using a similar argument by matrix Normal prior for $\tilde{\boldsymbol{\tau}}$, we have $\text{vec}(\tilde{\boldsymbol{\tau}})|\gamma_\tau, \eta_\tau \sim \mathcal{N}_{ND}(\mathbf{0}, \mathbf{I}_D \otimes \mathbf{K}_\tau)$. Therefore, we could use the elliptic slice sampler (ESS, Murray et al., 2010), which only requires the log-likelihood

$$\log p(\tilde{\boldsymbol{\tau}}; \tilde{\mathbf{Y}}, \tilde{\boldsymbol{\mu}}) = -M \mathbf{1}_{ND}^\top \text{vec}(\tilde{\boldsymbol{\tau}}) - \sum_{m=1}^M \frac{1}{2} \text{vec}(\mathbf{Y}_m^*)^\top \tilde{\mathbf{P}}_K^{-1} \text{vec}(\mathbf{Y}_m^*)$$

where $\tilde{\mathbf{P}}_K^{-1} := K_{(D,N)} \text{diag}(\{\tilde{\mathbf{P}}_n\})^{-1} K_{(N,D)}$ and $\mathbf{Y}_m^* := (\mathbf{Y}_m - \tilde{\boldsymbol{\mu}}) \circ \exp(-\tilde{\boldsymbol{\tau}})$.

($\tilde{\mathbf{L}}$). For each $n \in \{1, \dots, N\}$, we have $\text{vech}^\top(\mathbf{L}_n) \in \prod_{i=1}^D \mathcal{S}_0^{i-1}$. We could sample from its posterior distribution using the Δ -Spherical Hamiltonian Monte Carlo (Δ -SphHMC) described below. The log-posterior density of $\tilde{\mathbf{L}}$ is

$$\log p(\tilde{\mathbf{L}}|\tilde{\mathbf{Y}}, \tilde{\boldsymbol{\mu}}, \tilde{\boldsymbol{\tau}}, \gamma_L, \eta_L) = - \sum_{n=1}^N \left[M \log |\mathbf{L}_n| + \sum_{m=1}^M \frac{1}{2} \mathbf{y}_{mn}^* \mathbf{P}_n^{-1} \mathbf{y}_{mn}^* \right] - \frac{1}{2} \sum_{i=2}^D \text{tr}(\tilde{\mathbf{l}}_i^* \mathbf{K}_L^{-1} \tilde{\mathbf{l}}_i^*)$$

The derivative of log-likelihood with respect to \mathbf{L}_n and the derivative of log-prior with respect to $\tilde{\mathbf{l}}_i$ can be calculated as

$$\frac{\partial}{\partial \mathbf{L}_n} \log p(\tilde{\mathbf{L}}; \tilde{\mathbf{Y}}, \tilde{\boldsymbol{\mu}}, \tilde{\boldsymbol{\tau}}) = -M \frac{\mathbf{I}_D}{\mathbf{L}_n} + \sum_{m=1}^M \text{tril}(\mathbf{P}_n^{-1} \mathbf{y}_{mn}^* \mathbf{y}_{mn}^* \mathbf{P}_n^{-1} \mathbf{L}_n^{-\top}), \quad \frac{\partial}{\partial \tilde{\mathbf{l}}_i} \log p(\tilde{\mathbf{L}}|\gamma_L, \eta_L) = -\mathbf{K}_L^{-1} \tilde{\mathbf{l}}_i^*$$

D. SPHERICAL HAMILTONIAN MONTE CARLO

D.1. Derivation of the geometric integrator for SphHMC

The Lagrangian dynamics on the sphere $\mathcal{S}^{D-1}(r)$ with the first $(D-1)$ coordinates is

$$\begin{aligned} \dot{\mathbf{q}}_{-D} &= \mathbf{v}_{-D} \\ \dot{\mathbf{v}}_{-D} &= -\mathbf{v}_{-D}^\top \boldsymbol{\Gamma}(\mathbf{q}_{-D}) \mathbf{v}_{-D} - \mathbf{G}(\mathbf{q}_{-D})^{-1} \nabla_{\mathbf{q}_{-D}} \tilde{U}(\mathbf{q}) \end{aligned} \quad (\text{D.1})$$

where $\boldsymbol{\Gamma}(\mathbf{q}_{-D}) = r^{-2} \mathbf{G}(\mathbf{q}_{-D}) \otimes \mathbf{q}_{-D}$ is the Christoffel symbols of second kind (see details in Lan & Shahbaba, 2016, for $r = 1$). This dynamics (D.1) can be split into the following two smaller dynamics:

$$\begin{cases} \dot{\mathbf{q}}_{-D} = \mathbf{v}_{-D} \\ \dot{\mathbf{v}}_{-D} = -\mathbf{v}_{-D}^\top \boldsymbol{\Gamma}(\mathbf{q}_{-D}) \mathbf{v}_{-D} \end{cases} \quad (\text{D.2a}) \quad \begin{cases} \dot{\mathbf{q}}_{-D} = \mathbf{0} \\ \dot{\mathbf{v}}_{-D} = -\nabla_{\mathbf{q}_{-D}}^{-1} \tilde{U}(\mathbf{q}_{-D}) \end{cases} \quad (\text{D.2b})$$

where (D.2a) is the equation of geodesic on manifold \mathcal{S}^D which has analytical solution; and (D.2b) has analytical solution. Both define volume preserving maps.

The mapping $\mathcal{I} : \mathbf{q}_{-D} \mapsto \mathbf{q} = (\mathbf{q}_{-D}, q_D)$ can be viewed as an imbedding of \mathcal{S}_+^{D-1} into \mathbb{R}^D . Denote its Jacobian as $d\mathcal{I}(\mathbf{q}) := \begin{bmatrix} \mathbf{I}_{D-1} \\ \mathbf{q}_{-D}^\top \\ -\frac{\mathbf{q}_{-D}}{q_D} \end{bmatrix}$. Then we have

$$\begin{aligned} d\mathcal{I}(\mathbf{q})^\top d\mathcal{I}(\mathbf{q}) &= \mathbf{G}(\mathbf{q}_{-D}), & d\mathcal{I}(\mathbf{q})\mathbf{G}(\mathbf{q}_{-D})^{-1}d\mathcal{I}(\mathbf{q})^\top &= \mathcal{P}(\mathbf{q}) = \mathbf{I} - r^{-2}\mathbf{q}\mathbf{q}^\top \\ \nabla_{\mathbf{q}_{-D}}\tilde{U}(\mathbf{q}) &= d\mathcal{I}(\mathbf{q})^\top \nabla_{\mathbf{q}}\tilde{U}(\mathbf{q}), & \mathbf{v} &= d\mathcal{I}(\mathbf{q})\mathbf{v}_{-D}, & \mathbf{v}^\top \mathbf{v} &= \mathbf{v}_{-D}^\top \mathbf{G}(\mathbf{q}_{-D})\mathbf{v}_{-D} \end{aligned}$$

Then Equation (D.2a) has the following solution with full coordinates

$$\begin{aligned} \begin{bmatrix} \mathbf{q}(t) \\ \mathbf{v}(t) \end{bmatrix} &= \begin{bmatrix} \mathbf{I} & \mathbf{0} \\ \mathbf{0}^\top & r^{-1}\|\mathbf{v}(0)\|_2 \end{bmatrix} \begin{bmatrix} \cos(r^{-1}\|\mathbf{v}(0)\|_2 t) & \sin(r^{-1}\|\mathbf{v}(0)\|_2 t) \\ -\sin(r^{-1}\|\mathbf{v}(0)\|_2 t) & \cos(r^{-1}\|\mathbf{v}(0)\|_2 t) \end{bmatrix} \begin{bmatrix} \mathbf{I} & \mathbf{0} \\ \mathbf{0}^\top & r\|\mathbf{v}(0)\|_2^{-1} \end{bmatrix} \begin{bmatrix} \mathbf{q}(0) \\ \mathbf{v}(0) \end{bmatrix} \\ &= \begin{bmatrix} \mathbf{q}(0) \cos(r^{-1}\|\mathbf{v}(0)\|_2 t) + r\mathbf{v}(0)\|\mathbf{v}(0)\|_2^{-1} \sin(r^{-1}\|\mathbf{v}(0)\|_2 t) \\ -r^{-1}\mathbf{q}(0)\|\mathbf{v}(0)\|_2 \sin(r^{-1}\|\mathbf{v}(0)\|_2 t) + \mathbf{v}(0) \cos(r^{-1}\|\mathbf{v}(0)\|_2 t) \end{bmatrix} \end{aligned} \quad (\text{D.3})$$

and Equation (D.2b) has the following solution in full coordinates

$$\begin{aligned} \mathbf{q}(t) &= \mathbf{q}(0) \\ \mathbf{v}(t) &= \mathbf{v}(0) - \frac{t}{2} d\mathcal{I}(\mathbf{q}(0)) \nabla_{\mathbf{q}_{-D}}^{-1} \tilde{U}(\mathbf{q}(0)) = \mathbf{v}(0) - \frac{t}{2} \mathcal{P}(\mathbf{q}) \nabla_{\mathbf{q}} \tilde{U}(\mathbf{q}(0)) \end{aligned} \quad (\text{D.4})$$

So numerically updating (D.4) for $h/2$, updating (D.3) for h and updating (D.4) for another $h/2$ yield the integrator (11).

D.2. Reformulating Acceptance

At the end of the numerical simulation, a proposal $(\mathbf{q}_T, \mathbf{v}_T)$ is accepted according to the following probability

$$a_{sphHMC} = 1 \wedge \exp(-\Delta E), \quad \Delta E = E(\mathbf{q}_T, \mathbf{v}_T) - E(\mathbf{q}_0, \mathbf{v}_0) \quad (\text{D.5})$$

Such classic definition of acceptance probability can be reformulated by replacing ΔE in (D.5) with

$$\Delta E = \sum_{\tau=1}^T \Delta E_\tau \quad \Delta E_\tau = E(\mathbf{q}_\tau, \mathbf{v}_\tau) - E(\mathbf{q}_{\tau-1}, \mathbf{v}_{\tau-1})$$

With (11) we can write

$$\begin{aligned} \Delta E' &= E(\mathbf{q}', \mathbf{v}') - E(\mathbf{q}, \mathbf{v}) \\ &= \tilde{U}(\mathbf{q}') - \tilde{U}(\mathbf{q}) + \frac{1}{2} \mathbf{v}'^\top \mathbf{G}(\mathbf{q}'_{-D}) \mathbf{v}'_{-D} - \frac{1}{2} \mathbf{v}^\top \mathbf{G}(\mathbf{q}_{-D}) \mathbf{v}_{-D} \\ &= \Delta \tilde{U} - \frac{1}{2} \|\mathbf{v}\|_2^2 + \frac{1}{2} \left\| \mathbf{v}^+ - \frac{h}{2} \mathcal{P}(\mathbf{q}') \nabla_{\mathbf{q}} \tilde{U}(\mathbf{q}') \right\|_2^2 \\ &= \Delta \tilde{U} - \frac{1}{2} \|\mathbf{v}\|_2^2 + \frac{1}{2} \mathbf{v}^{+\top} \mathbf{v}^+ - \frac{h}{2} \mathbf{v}^{+\top} \mathcal{P}(\mathbf{q}') \nabla_{\mathbf{q}} \tilde{U}(\mathbf{q}') + \frac{h^2}{8} \nabla_{\mathbf{q}} \tilde{U}(\mathbf{q}')^\top \mathcal{P}(\mathbf{q}') \nabla_{\mathbf{q}} \tilde{U}(\mathbf{q}') \\ &= \Delta \tilde{U} - \frac{1}{2} \|\mathbf{v}\|_2^2 + \frac{1}{2} \|\mathbf{v}^-\|_2^2 - \frac{h}{2} \mathbf{v}^{+\top} \nabla_{\mathbf{q}} \tilde{U}(\mathbf{q}') + \frac{h^2}{8} \|\nabla_{\mathbf{q}} \tilde{U}(\mathbf{q}')\|_{\mathcal{P}(\mathbf{q}')}^2 \\ &= \Delta \tilde{U} - \frac{1}{2} \|\mathbf{v}\|_2^2 - \frac{h}{2} \mathbf{v}^{+\top} \nabla_{\mathbf{q}} \tilde{U}(\mathbf{q}') + \frac{h^2}{8} \|\nabla_{\mathbf{q}} \tilde{U}(\mathbf{q}')\|_{\mathcal{P}(\mathbf{q}')}^2 + \frac{1}{2} \|\mathbf{v}\|_2^2 - \frac{h}{2} \mathbf{v}^\top \nabla_{\mathbf{q}} \tilde{U}(\mathbf{q}) + \frac{h^2}{8} \|\nabla_{\mathbf{q}} \tilde{U}(\mathbf{q})\|_{\mathcal{P}(\mathbf{q})}^2 \\ &= \Delta \tilde{U} - \frac{h}{2} \left[\mathbf{v}'^\top \nabla_{\mathbf{q}} \tilde{U}(\mathbf{q}') + \mathbf{v}^\top \nabla_{\mathbf{q}} \tilde{U}(\mathbf{q}) \right] - \frac{h^2}{8} \left[\|\nabla_{\mathbf{q}} \tilde{U}(\mathbf{q}')\|_{\mathcal{P}(\mathbf{q}')}^2 - \|\nabla_{\mathbf{q}} \tilde{U}(\mathbf{q})\|_{\mathcal{P}(\mathbf{q})}^2 \right] \end{aligned}$$

where $\mathcal{P}(\mathbf{q}')\mathbf{v}^+ = \mathbf{v}^+$, $\mathcal{P}(\mathbf{q})\mathbf{v}^- = \mathbf{v}^-$, and $\|\mathbf{v}^+\|_2^2 = \|\mathbf{v}^-\|_2^2$. Accumulating the above terms over $\tau = 1, \dots, T$ yields the reformulated acceptance probability (12).

Algorithm 1. Adaptive Spherical HMC (adp-SphHMC)

Given $\mathbf{q}_0, a_0, N, N^{adapt}$.
Set $h_0 = 1$ or using Algorithm 4 of Hoffman & Gelman (2014),
 $\mu = \log(10h_0), \bar{h}_0 = 1, \bar{A}_0 = 0, \gamma = 0.05, n_0 = 10, \kappa = 0.75$.
for $n = 1$ to N **do**
 Sample a new velocity $\mathbf{v}_{n-1} \sim \mathcal{N}(\mathbf{0}, \mathbf{I}_D)$, and set $\mathbf{v}_{n-1} = \mathcal{P}(\mathbf{q}_{n-1})\mathbf{v}_{n-1}$.
 Set $\mathbf{q}^{(0)} = \mathbf{q}_{n-1}, \mathbf{v}^{(0)} = \mathbf{v}_{n-1}$.
 for $\tau = 0$ to $T - 1$ ($T = T_{2orth}$ or T_{stoch}) **do**
 Run leapfrog step (11) to update $(\mathbf{q}^{(\tau+1)}, \mathbf{v}^{(\tau+1)}) \leftarrow \mathcal{T}_{\bar{h}_{n-1}}(\mathbf{q}^{(\tau)}, \mathbf{v}^{(\tau)})$.
 if Stopping criterion (D.6) (or (D.7)) is satisfied **then**
 Break
 end if
 end for
 Accept the proposal $(\mathbf{q}^{(T)}, \mathbf{v}^{(T)})$ with probability a_n^{sphHMC} in (12) and set $\mathbf{q}_n = \mathbf{q}^{(T)}$; otherwise set
 $\mathbf{q}_n = \mathbf{q}_{n-1}$.
 if $n \leq N^{adapt}$ **then**
 Set $\bar{A}_n = \left(1 - \frac{1}{n+n_0}\right)\bar{A}_{n-1} + \frac{1}{n+n_0}(a_0 - a_n)$.
 Set $\log h_n = \mu - \frac{\sqrt{n}}{\gamma}\bar{A}_n$, and $\log \bar{h}_n = n^{-\kappa} \log h_n + (1 - n^{-\kappa}) \log \bar{h}_{n-1}$.
 else
 Set $h_n = \bar{h}_{N^{adapt}}$.
 end if
end for

D.3. Adaptive Spherical HMC

There are two tuning parameters in HMC and its variants: the step size h and the number of integration (leapfrog) steps T . Hand tuning heavily relies on domain expertise and could be inefficient. Here, we adopt the ‘No-U-Turn’ idea from Hoffman & Gelman (2014) and introduce a novel adaptive algorithm that obviates manual tuning of these parameters.

First, for any given step size h , we adopt a rule for setting the number of leapfrog steps based on the same philosophy as ‘No-U-Turn’ (Hoffman & Gelman, 2014). The idea is to avoid waste of computation occurred (e.g. when the sampler backtracks on its trajectory) without breaking the detailed balance condition for the MCMC transition kernel. $S^{D-1}(r)$ is a compact manifold where any two points $\mathbf{q}(0), \mathbf{q}(t) \in S^{D-1}(r)$ have bounded geodesic distance πr . We adopt the stopping rule for the leapfrog when the sampler exits the orthant of the initial state, that is, the trajectory measured in geodesic distance is at least $\frac{\pi}{2}r$, which is equivalent to $\langle \mathbf{q}(0), \mathbf{q}(t) \rangle < 0$. On the other hand, this condition may not be satisfied within reasonable number of iterations because the geometric integrator (11) does not follow a geodesic (great circle) in general (only the middle part does), therefore we set some threshold T_{\max} for the number of tests, and adopt the following ‘Two-Orthants’ (as the starting and end points occupy two orthants) rule for the number of leapfrogs:

$$T_{2orth} = \min_{\tau \in \{0, \dots, T_{\max}\}} \{\tau : \langle \mathbf{q}_0, \mathbf{q}_\tau \rangle < 0\} \quad (\text{D.6})$$

Alternatively, one can stop the leapfrog steps in a *stochastic* way based on the geodesic distance travelled:

$$T_{stoch} = \min_{\tau} \{\tau : Z_\tau = 0\}, \quad Z_\tau \sim \text{Bern}(p_\tau), \quad p_\tau = \frac{r^{-2} \langle \mathbf{q}_0, \mathbf{q}_\tau \rangle + 1}{2} \quad (\text{D.7})$$

These stopping criteria are already time reversible, so the recursive binary tree as in ‘No-U-Turn’ algorithm (Hoffman & Gelman, 2014) is no longer needed.

Lastly, we adopt the *dual averaging* scheme (Nesterov, 2009) for the adaptation of step size h . See Hoffman & Gelman (2014) for more details. We summarize our *Adaptive Spherical Hamiltonian Monte Carlo* (adp-SphHMC) in Algorithm 1.

We now prove the energy conservation theorem 4 (Beskos et al., 2011).

Proof of Theorem 4. With the second equation of Lagrangian dynamics (D.1) we have

$$\begin{aligned}
 -\langle \mathbf{v}(t), \mathbf{g}(\mathbf{q}(t)) \rangle &= \mathbf{v}(t)^\top \nabla_{\mathbf{q}} \tilde{U}(\mathbf{q}(t)) = \mathbf{v}_{-D}(t)^\top d\mathcal{I}(\mathbf{q})^\top \nabla_{\mathbf{q}} \tilde{U}(\mathbf{q}(t)) = \mathbf{v}_{-D}(t)^\top \nabla_{\mathbf{q}_{-D}} \tilde{U}(\mathbf{q}(t)) \\
 &= \mathbf{v}_{-D}(t)^\top \mathbf{G}(\mathbf{q}_{-D}(t)) [\dot{\mathbf{v}}_{-D}(t) + \mathbf{v}_{-D}(t)^\top \mathbf{\Gamma}(\mathbf{q}_{-D}(t)) \mathbf{v}_{-D}(t)] \\
 &= \mathbf{v}_{-D}(t)^\top \mathbf{G}(\mathbf{q}_{-D}(t)) \dot{\mathbf{v}}_{-D}(t) + \frac{1}{2} \mathbf{v}_{-D}(t)^\top d\mathbf{G}(\mathbf{q}_{-D}(t)) \mathbf{v}_{-D}(t) \\
 &= \frac{d}{dt} \frac{1}{2} \mathbf{v}_{-D}(t)^\top \mathbf{G}(\mathbf{q}_{-D}(t)) \mathbf{v}_{-D}(t) = \frac{d}{dt} \frac{1}{2} \|\mathbf{v}(t)\|_2^2
 \end{aligned}$$

Then we have the first equality hold because

$$-\int_0^T \langle \mathbf{v}(t), \mathbf{g}(\mathbf{q}(t)) \rangle dt = \frac{1}{2} \|\mathbf{v}(T)\|_2^2 - \frac{1}{2} \|\mathbf{v}(0)\|_2^2$$

Lastly, from the first equation of Lagrangian dynamics (D.1)

$$\tilde{U}(\mathbf{q}(T)) - \tilde{U}(\mathbf{q}(0)) = \int_0^T \dot{\tilde{U}}(\mathbf{q}(t)) dt = \int_0^T \langle \dot{\mathbf{q}}(t), \nabla_{\mathbf{q}} \tilde{U}(\mathbf{q}(t)) \rangle dt = \int_0^T \langle \mathbf{v}(t), \mathbf{g}(\mathbf{q}(t)) \rangle dt$$

Therefore the second equality is proved. \square

E. GRADIENT CALCULATION IN NORMAL-INVERSE-WISHART PROBLEM

We use the representation (4) and derive log-posterior (log-likelihood and log-prior) and the corresponding gradients for (13) using matrix calculus.

E.1. Gradients of log-likelihood

Denote $\mathbf{y}_n^* := (\mathbf{y}_n - \boldsymbol{\mu}_0)/\boldsymbol{\sigma}$. Then the log-likelihood becomes

$$\ell(\mathbf{y}^*; \boldsymbol{\sigma}, \mathbf{P}) = -N \mathbf{1}_D^\top \log \boldsymbol{\sigma} - \frac{N}{2} \log |\mathbf{P}| - \frac{1}{2} \sum_{n=1}^N \mathbf{y}_n^{*\top} \mathbf{P}^{-1} \mathbf{y}_n^*$$

$\left[\frac{\partial \ell}{\partial \boldsymbol{\tau}}\right]$. We calculate the gradient of log-likelihood with respect to $\boldsymbol{\sigma}$

$$\frac{\partial \ell}{\partial \sigma_k} = -N \sigma_k^{-1} + \sum_{n=1}^N \sum_i \frac{y_{ni}^*}{\sigma_i} \delta_{ik} (\mathbf{P}^{-1} \mathbf{y}_n^*)_i, \quad i.e. \quad \frac{\partial \ell}{\partial \boldsymbol{\sigma}} = -N \boldsymbol{\sigma}^{-1} + \sum_{n=1}^N \text{diag}(\mathbf{y}_n^*/\boldsymbol{\sigma}) (\mathbf{P}^{-1} \mathbf{y}_n^*)$$

And with the transformation $\boldsymbol{\tau} = \log(\boldsymbol{\sigma})$ it becomes

$$\frac{\partial \ell}{\partial \boldsymbol{\tau}} = \frac{d\boldsymbol{\sigma}^\top}{d\boldsymbol{\tau}} \frac{\partial \ell}{\partial \boldsymbol{\sigma}} = \text{diag}(\boldsymbol{\sigma}) \left[-\frac{N}{\boldsymbol{\sigma}} + \sum_{n=1}^N \text{diag}(\mathbf{y}_n^*/\boldsymbol{\sigma}) (\mathbf{P}^{-1} \mathbf{y}_n^*) \right] = -N \mathbf{1}_D + \sum_{n=1}^N \text{diag}(\mathbf{y}_n^*) (\mathbf{P}^{-1} \mathbf{y}_n^*)$$

$\left[\frac{\partial \ell}{\partial \mathbf{U}^*} \left(\frac{\partial \ell}{\partial \mathbf{L}} \right)\right]$. When $\mathbf{P} = \mathbf{U}^* (\mathbf{U}^*)^\top$, $\frac{1}{2} \log |\mathbf{P}| = \log |\mathbf{U}^*| = \mathbf{1}_D^\top \log |\text{diag}(\mathbf{U}^*)|$ and thus we have

$$\frac{\partial \ell}{\partial \mathbf{U}^*} = -\frac{N \mathbf{I}_D}{\mathbf{U}^*} + \sum_{n=1}^N \frac{dg_n(\tilde{\mathbf{U}})}{d\mathbf{U}^*}$$

where $\frac{\mathbf{I}_D}{\mathbf{U}^*} = \text{diag}(\{(u_{ii}^*)^{-1}\})$ is a diagonal matrix formed by element-wise division, $\tilde{\mathbf{U}} := (\mathbf{U}^*)^{-1}$ and $g_n(\tilde{\mathbf{U}}) := -\frac{1}{2} \mathbf{y}_n^{*\top} \tilde{\mathbf{U}}^\top \tilde{\mathbf{U}} \mathbf{y}_n^*$.

Taking differential directly on $g_n(\mathbf{U}^*) := -\frac{1}{2}\mathbf{y}_n^{*\top}(\mathbf{U}^*)^{-\top}(\mathbf{U}^*)^{-1}\mathbf{y}_n^*$, and noting that differential and trace operators are exchangeable, we have

$$\begin{aligned} dg_n(\mathbf{U}^*) &= -\frac{1}{2}\text{tr}(\mathbf{y}_n^{*\top}d(\mathbf{U}^*)^{-\top}(\mathbf{U}^*)^{-1}\mathbf{y}_n^* + \mathbf{y}_n^{*\top}(\mathbf{U}^*)^{-\top}d(\mathbf{U}^*)^{-1}\mathbf{y}_n^*) \\ &= \frac{1}{2}\left[\text{tr}(\mathbf{y}_n^{*\top}(\mathbf{U}^*)^{-\top}d(\mathbf{U}^*)^{\top}\mathbf{P}^{-1}\mathbf{y}_n^*) + \text{tr}(\mathbf{y}_n^{*\top}\mathbf{P}^{-1}d\mathbf{U}^*(\mathbf{U}^*)^{-1}\mathbf{y}_n^*)\right] \\ &= \text{tr}(\mathbf{y}_n^{*\top}\mathbf{P}^{-1}d\mathbf{U}^*(\mathbf{U}^*)^{-1}\mathbf{y}_n^*) = \text{tr}((\mathbf{U}^*)^{-1}\mathbf{y}_n^*\mathbf{y}_n^{*\top}\mathbf{P}^{-1}d\mathbf{U}^*) \end{aligned}$$

Conversion from differential to normal derivative form in the numerator layout (Minka, 1997; revised 12/00) yields

$$\frac{\partial g_n(\mathbf{U}^*)}{\partial(\mathbf{U}^*)^{\top}} = \text{tril}((\mathbf{U}^*)^{-1}\mathbf{y}_n^*\mathbf{y}_n^{*\top}\mathbf{P}^{-1}), \quad i.e., \quad \frac{\partial g_n(\mathbf{U}^*)}{\partial\mathbf{U}^*} = \text{triu}(\mathbf{P}^{-1}\mathbf{y}_n^*\mathbf{y}_n^{*\top}(\mathbf{U}^*)^{-\top})$$

Finally, we have

$$\frac{\partial \ell}{\partial\mathbf{U}^*} = -\frac{N\mathbf{I}_D}{\mathbf{U}^*} + \text{triu}(\mathbf{P}^{-1}\sum_{n=1}^N\mathbf{y}_n^*\mathbf{y}_n^{*\top}(\mathbf{U}^*)^{-\top})$$

When $\mathbf{P} = \mathbf{L}\mathbf{L}^{\top}$, by similar argument as above, we have

$$\frac{\partial \ell}{\partial\mathbf{L}} = -\frac{N\mathbf{I}_D}{\mathbf{L}} + \text{tril}(\mathbf{P}^{-1}\sum_{n=1}^N\mathbf{y}_n^*\mathbf{y}_n^{*\top}\mathbf{L}^{-\top})$$

E.2. Gradients of log-priors

The logarithm of conditional prior $p(\boldsymbol{\sigma}|\mathbf{U}^*)$ after transformation $\boldsymbol{\tau} = \log(\boldsymbol{\sigma})$ becomes

$$\log p(\boldsymbol{\tau}|\mathbf{U}^*) = \log p(\boldsymbol{\sigma}|\mathbf{U}^*) + \log \left| \frac{d\boldsymbol{\sigma}}{d\boldsymbol{\tau}} \right| = \sum_{i=1}^D (i - (\nu + D))\tau_i - \frac{1}{2}\text{tr}(\boldsymbol{\Psi} \text{diag}(e^{-\boldsymbol{\tau}})\mathbf{P}^{-1} \text{diag}(e^{-\boldsymbol{\tau}}))$$

$\left[\frac{d}{d\boldsymbol{\tau}} \log p(\boldsymbol{\tau}|\mathbf{U}^*)\right]$. We calculate the derivative of $\log p(\boldsymbol{\tau}|\mathbf{U}^*)$ with respect to $\boldsymbol{\tau}$

$$\frac{d}{d\boldsymbol{\tau}} \log p(\boldsymbol{\tau}|\mathbf{U}^*) = \mathbf{i} - (\nu + D) + \frac{dg(\boldsymbol{\tau})}{d\boldsymbol{\tau}}$$

where $\mathbf{i} = [1, \dots, D]^{\top}$, and $g(\boldsymbol{\tau}) = -\frac{1}{2}\text{tr}(\boldsymbol{\Psi} \text{diag}(e^{-\boldsymbol{\tau}})\mathbf{P}^{-1} \text{diag}(e^{-\boldsymbol{\tau}}))$.

Noting that differential and trace operators are exchangeable, we have

$$\begin{aligned} dg(\boldsymbol{\tau}) &= -\frac{1}{2}\text{tr}(\boldsymbol{\Psi}d \text{diag}(e^{-\boldsymbol{\tau}})\mathbf{P}^{-1} \text{diag}(e^{-\boldsymbol{\tau}}) + \boldsymbol{\Psi} \text{diag}(e^{-\boldsymbol{\tau}})\mathbf{P}^{-1}d \text{diag}(e^{-\boldsymbol{\tau}})) \\ &= \frac{1}{2}\left[\text{tr}(\mathbf{P}^{-1} \text{diag}(e^{-\boldsymbol{\tau}})\boldsymbol{\Psi} \text{diag}(e^{-\boldsymbol{\tau}}) \text{diag}(d\boldsymbol{\tau})) + \text{tr}(\boldsymbol{\Psi} \text{diag}(e^{-\boldsymbol{\tau}})\mathbf{P}^{-1} \text{diag}(e^{-\boldsymbol{\tau}}) \text{diag}(d\boldsymbol{\tau}))\right] \\ &= \sum_{i=1}^D d\tau_i \sum_{j=1}^D \psi_{ij}e^{-\tau_j} \rho^{ji}e^{-\tau_i} \end{aligned}$$

Thus

$$\frac{dg(\boldsymbol{\tau})}{d\boldsymbol{\tau}} = \text{diag}(\boldsymbol{\Psi} \text{diag}(e^{-\boldsymbol{\tau}})\mathbf{P}^{-1}) \text{diag}(e^{-\boldsymbol{\tau}}) = \text{diag}(\boldsymbol{\Psi} \text{diag}(e^{-\boldsymbol{\tau}})\mathbf{P}^{-1}) \circ e^{-\boldsymbol{\tau}}$$

where diag acting on a vector forms a diagonal matrix while the action a matrix means extracting the diagonal vector. \circ is the Hadamard product (a.k.a. Schur product), i.e. the entrywise product.

$\left[\frac{d}{d\mathbf{U}^*} \log p(\mathbf{U}^*|\boldsymbol{\tau})\right]$. Now consider the derivative of $\log p(\mathbf{U}^*|\boldsymbol{\tau})$ with respect to the matrix \mathbf{U}^* . We have

$$\frac{d}{d\mathbf{U}^*} \log p(\mathbf{U}^*|\boldsymbol{\tau}) = \frac{\text{diag}(\mathbf{i} - (\nu + D + 1))}{\mathbf{U}^*} + \frac{dg(\mathbf{U}^*)}{d\mathbf{U}^*}$$

where $g(\mathbf{U}^*) = -\frac{1}{2}\text{tr}(\Psi \text{diag}(e^{-\tau})(\mathbf{U}^*)^{-\top}(\mathbf{U}^*)^{-1} \text{diag}(e^{-\tau}))$, and $\frac{\text{diag}(\mathbf{i})}{\mathbf{U}^*}$ is a diagonal matrix formed by element-wise division.

Again by the exchangeability between differential and trace, we have

$$\begin{aligned} dg(\mathbf{U}^*) &= -\frac{1}{2}\text{tr}(\Psi \text{diag}(e^{-\tau})d(\mathbf{U}^*)^{-\top}(\mathbf{U}^*)^{-1} \text{diag}(e^{-\tau}) + \Psi \text{diag}(e^{-\tau})(\mathbf{U}^*)^{-\top}d(\mathbf{U}^*)^{-1} \text{diag}(e^{-\tau})) \\ &= \frac{1}{2}\left[\text{tr}(\Psi \text{diag}(e^{-\tau})(\mathbf{U}^*)^{-\top}d(\mathbf{U}^*)^{\top}\mathbf{P}^{-1} \text{diag}(e^{-\tau})) + \text{tr}(\Psi \text{diag}(e^{-\tau})\mathbf{P}^{-1}d\mathbf{U}^*(\mathbf{U}^*)^{-1} \text{diag}(e^{-\tau}))\right] \\ &= \frac{1}{2}\left[\text{tr}(\text{diag}(e^{-\tau})\mathbf{P}^{-1}d\mathbf{U}^*(\mathbf{U}^*)^{-1} \text{diag}(e^{-\tau})\Psi) + \text{tr}(\Psi \text{diag}(e^{-\tau})\mathbf{P}^{-1}d\mathbf{U}^*(\mathbf{U}^*)^{-1} \text{diag}(e^{-\tau}))\right] \\ &= \text{tr}((\mathbf{U}^*)^{-1} \text{diag}(e^{-\tau})\Psi \text{diag}(e^{-\tau})\mathbf{P}^{-1}d\mathbf{U}^*) \end{aligned}$$

Therefore we have

$$\frac{dg(\mathbf{U}^*)}{d(\mathbf{U}^*)^{\top}} = \text{tril}((\mathbf{U}^*)^{-1} \text{diag}(e^{-\tau})\Psi \text{diag}(e^{-\tau})\mathbf{P}^{-1}),$$

that is,

$$\frac{dg(\mathbf{U}^*)}{d\mathbf{U}^*} = \text{triu}(\mathbf{P}^{-1} \text{diag}(e^{-\tau})\Psi \text{diag}(e^{-\tau})(\mathbf{U}^*)^{-\top}),$$

$\left[\frac{d}{d\tau} \log p(\tau), \frac{d}{d\mathbf{L}} \log p(\mathbf{L})\right]$. Lastly, the log-priors for (15) and their gradients after transformation $\tau := \log(\sigma)$ are calculated

$$\begin{aligned} \log p(\tau) &= -\frac{1}{2}\tau^{\top}\tau, & \frac{d}{d\tau} \log p(\tau) &= -\tau \\ \log p(\mathbf{l}_i) &= \log p(\mathbf{l}_i^2) + \mathbf{1}_i^{\top} \log |2\mathbf{l}_i| = (2\alpha_i - 1) + \mathbf{1}_i^{\top} \log |\mathbf{l}_i|, & \frac{d}{d\mathbf{l}_i} \log p(\mathbf{l}_i) &= \frac{2(\alpha_i - 1) + \mathbf{1}_i}{\mathbf{l}_i} \end{aligned}$$

The bottom row can be written as

$$\log p(\mathbf{L}) = \sum_{i=1}^D (2\alpha_i - 1)^{\top} \log |\mathbf{l}_i|, \quad \frac{d}{d\mathbf{L}} \log p(\mathbf{L}) = \frac{2\alpha - 1}{\mathbf{L}}$$

where $\frac{1}{\mathbf{L}}$ denotes a lower-triangular matrix with l_{ij}^{-1} being its (i, j) entry ($i \geq j$).

F. MORE NUMERICAL RESULTS

F.1. Flexibility of von Mises-Fisher Prior and Bingham Prior

Definition F.1 (Fisher-Bingham / Kent distribution). The probability density function of the Kent distribution for the random vector $\mathbf{l}_i \in \mathcal{S}^{i-1}$ is given by

$$p(\mathbf{l}_i) \propto \exp \left\{ \kappa \gamma_1^{\top} \mathbf{l}_i + \sum_{k=2}^i \beta_k (\gamma_k^{\top} \mathbf{l}_i)^2 \right\}$$

where $\sum_{k=2}^i \beta_k = 0$ and $0 \leq 2|\beta_k| < \kappa$ and the vectors $\{\gamma_k\}_{k=1}^i$ are orthonormal. \square

Remark F.1. The parameters κ and γ_1 are called the *concentration* and the *mean direction* parameter, respectively. The greater the value of κ , the higher the concentration of the distribution around the mean direction γ_1 . The choice of γ_1 could impact our priors when modeling correlations. Parameters $\{\beta_k\}_{k=2}^i$ determine the ellipticity of the contours of equal probability. The vectors $\{\gamma_k\}_{k=2}^i$ determine the orientation of the equal probability contours on the sphere. \square

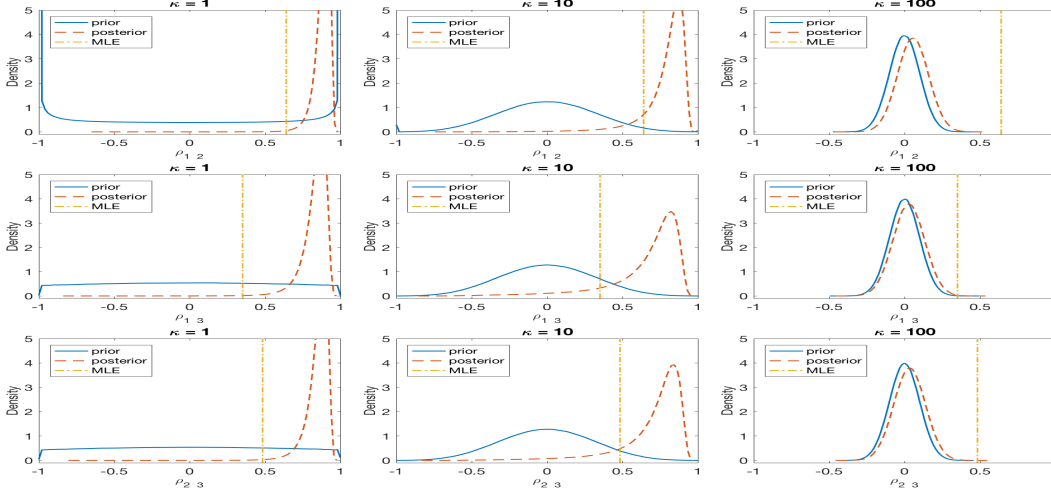


Fig. F.1: Marginal posterior, prior (induced from von Mises-Fisher distribution) densities of correlations and MLEs with different settings for concentration parameter κ , estimated with 10^6 samples.

Remark F.2. If $\beta_k = 0$ for $k = 2, \dots, i$, then this distribution reduces to *von Mises-Fisher* distribution (Fisher, 1953; Mardia & Jupp, 2009), denoted as $\text{vMF}(\kappa, \gamma_1)$. If $\kappa = 0$, then it defines an antipodally symmetric distribution, named *Bingham* distribution (Bingham, 1974), denoted as $\text{Bing}(\mathbf{A})$, with $\mathbf{l}_i^\top \mathbf{A} \mathbf{l}_i = \sum_{k=2}^i \beta_k (\gamma_k^\top \mathbf{l}_i)^2$. \square

As before, to induce smaller correlations, one can put higher prior probabilities for \mathbf{l}_i on the poles of \mathcal{S}^{i-1} . For example, we might consider $\mathbf{l}_i \sim \text{vMF}(\kappa, \mathbf{n}_i)$, or $\mathbf{l}_i \sim \text{Bing}(\zeta \text{diag}(\mathbf{n}_i))$, where $\mathbf{n}_i := (0, \dots, 0, 1)^\top$ is denoted as the north pole. Now let's consider the following von Mises-Fisher prior (Fisher et al., 1987; Fisher, 1953; Mardia & Jupp, 2009) for \mathbf{l}_i , the i -th row of the Cholesky factor \mathbf{L} of correlation matrix \mathbf{P} in the structured model (4).

Definition F.2 (Von Mises-Fisher distribution). The probability density function of the von Mises-Fisher distribution for the random vector $\mathbf{l}_i \in \mathcal{S}^{i-1}$ is given by

$$p(\mathbf{l}_i) = C_i(\kappa) \exp(\kappa \boldsymbol{\mu}^\top \mathbf{l}_i)$$

where $\kappa \geq 0$, $\|\boldsymbol{\mu}\| = 1$ and the normalization constant $C_i(\kappa)$ is equal to

$$C_i(\kappa) = \frac{\kappa^{i/2-1}}{(2\pi)^{i/2} I_{i/2-1}(\kappa)}$$

where I_v denotes the modified *Bessel* function of the first kind at order v . Denote $\mathbf{l}_i \sim \text{vMF}(\kappa, \boldsymbol{\mu})$. \square

Since we have no prior knowledge about the mean direction $\boldsymbol{\mu}$, we choose $\boldsymbol{\mu} = \mathbf{n}_i = (\mathbf{0}_{i-1}, 1)^\top$ that favors the polar direction, i.e.

$$\mathbf{l}_i \sim \text{vMF}(\kappa, \mathbf{n}_i), \quad p(\mathbf{l}_i) \propto \exp(\kappa l_{ii}), \quad i = 2, \dots, D$$

where we consider i) $\kappa = 1$; ii) $\kappa = 10$; iii) $\kappa = 100$. With the von Mises-Fisher prior, we have

$$\log p(\mathbf{L}) = \sum_{i=1}^D \kappa l_{ii} = \kappa \text{tr}(\mathbf{L}), \quad \frac{d}{d\mathbf{L}} \log p(\mathbf{L}) = \kappa \mathbf{I}$$

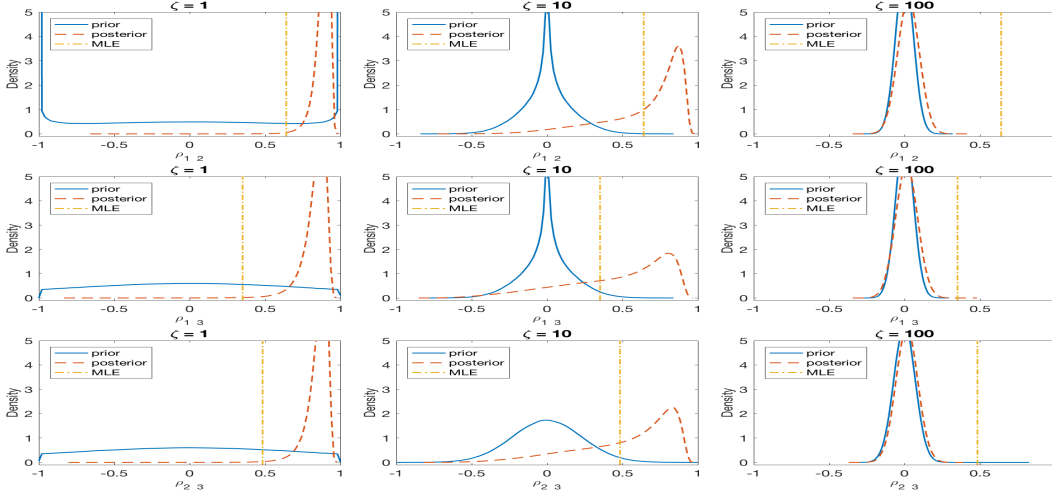


Fig. F.2: Marginal posterior, prior (induced from Bingham distribution) densities of correlations and MLEs with different settings for concentration parameter ζ , estimated with 10^6 samples.

With the von Mises–Fisher prior for \mathbf{l}_i , the posteriors, priors and maximal likelihood estimates (MLE) of correlations with different κ 's are plotted in Figure F.1 respectively. With larger concentration parameter κ , the posterior is pulled more towards 0.

Finally, we consider the following Bingham prior (Bingham, 1974; Onstott, 1980) for \mathbf{l}_i in the structured model (4).

Definition F.3 (Bingham distribution). The probability density function of the Bingham distribution for the random vector $\mathbf{l}_i \in \mathcal{S}^{i-1}$ is given by

$$p(\mathbf{l}_i) = {}_1F_1\left(\frac{1}{2}; \frac{n}{2}; \mathbf{Z}\right)^{-1} \exp(\mathbf{l}_i^\top \mathbf{M} \mathbf{Z} \mathbf{M}^\top \mathbf{l}_i)$$

where \mathbf{M} is an orthogonal orientation matrix, \mathbf{Z} is a diagonal concentration matrix, and ${}_1F_1(\cdot; \cdot; \cdot)$ is a *confluent hypergeometric function* of matrix argument. Denote $\mathbf{l}_i \sim \text{Bing}(\mathbf{M}, \mathbf{Z})$. \square

Note, according to Bingham (1974), this distribution is defined for \mathbf{Z} up to an arbitrary scalar matrix $\zeta_0 \mathbf{I}$. Therefore, we consider $\mathbf{M} = \mathbf{I}$ and $\mathbf{Z} = \zeta \text{diag}(\mathbf{n}_i)$ that favors the polar direction, i.e.

$$\mathbf{l}_i \sim \text{Bing}(\mathbf{I}, \zeta \text{diag}(\mathbf{n}_i)), \quad p(\mathbf{l}_i) \propto \exp(\zeta l_{ii}^2), \quad i = 2, \dots, D$$

where we consider i) $\zeta = 1$; ii) $\zeta = 10$; iii) $\zeta = 100$. The log-prior and its gradient are calculated as follows

$$\log p(\mathbf{L}) = \sum_{i=1}^D \zeta l_{ii}^2 = \zeta \|\text{diag}(\mathbf{L})\|^2, \quad \frac{d}{d\mathbf{L}} \log p(\mathbf{L}) = 2\zeta \text{diag}(\mathbf{L})$$

We repeat the above experiment with the Bingham prior for \mathbf{l}_i . The posteriors, priors and maximal likelihood estimates (MLE) of correlations with different ζ 's are plotted in Figure F.2 respectively. With larger concentration parameter ζ , the posteriors are pulled more towards the induced priors and concentrate on 0.

F.2. More Comparison to Latent Factor Process Model

The example of simulated periodic process in Section 4.2 is consider for $D = 2$ for simplicity and convenience of visualization. Here we consider higher dimension $D = 10$. The purpose here is not to

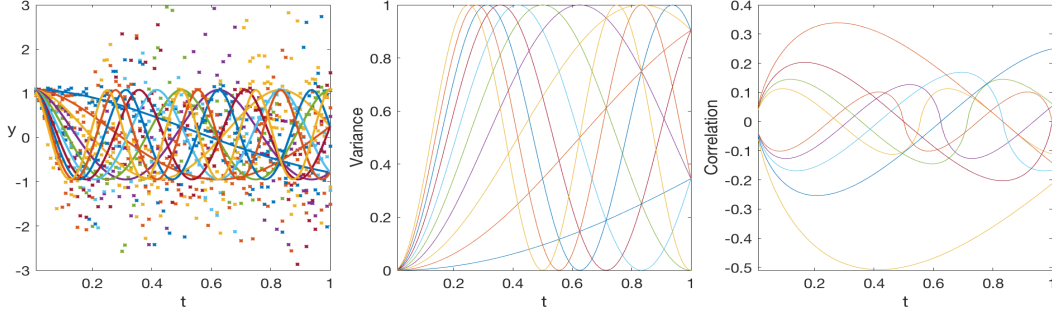


Fig. F.3: Simulated data y over the underlying mean functions μ_t (left), the variance functions Σ_t , and the correlation functions P_t (right) of 10-dimension periodic processes.

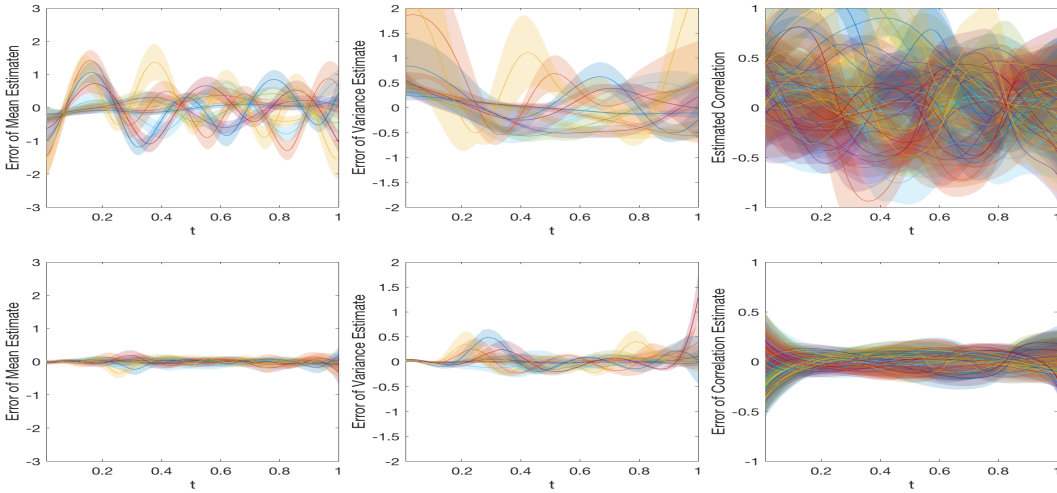


Fig. F.4: Estimated error functions of the underlying mean μ_t (left column), variance σ_t (middle column) and correlation ρ_t (right column) of 10-dimensional periodic processes, using latent factor process model (upper row) and our flexible model (lower row), based on $M = 20$ trials of data over $N = 100$ evenly spaced points. Solid lines are estimated errors and shaded regions are 95% credible bands.

show the scalability, but rather to investigate the robustness of our dynamic model (8) in terms of full flexibility.

We generate $M = 20$ trials of data over $N = 100$ evenly spaced points over $[0, 1]$. The true mean, variance and correlation functions are modified from the example (16) using the Clausen functions (Clausen, 1832). Seen from Figure F.3, they behave more intricately with higher heterogeneity among those processes. This could impose further challenge for latent factor based models like (17) compared to $D = 2$. We repeat the experiments in Section 4.2 and compare our dynamic model (8) with the latent factor process model (17) by Fox & Dunson (2015). To aid the visualization, we subtract the estimated process from their true values and plot the error functions in Figure F.4. Even if we have tried our best to tune the parameters, e.g. L , the number of basis functions, and k , the size of latent factors, the latent factor process model (Fox & Dunson, 2015) is outperformed by our flexible dynamic model (8) in reducing estimation errors.

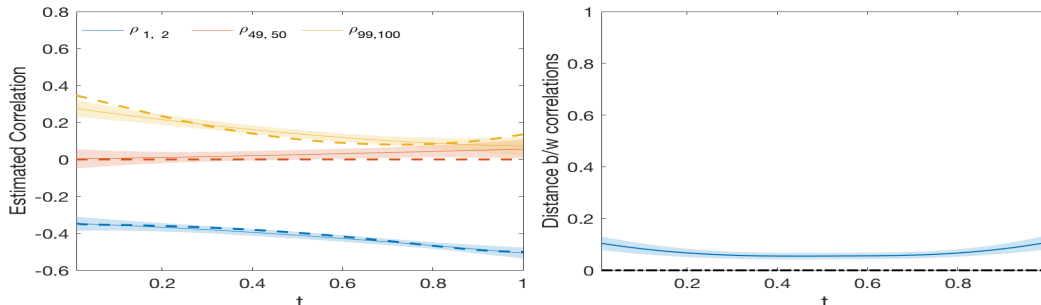


Fig. F.5: Posterior estimation of the underlying correlation functions P_t (left) and its 2-norm distance to the truth (right) of 100-dimensional periodic processes with 2-band structure, based on $M = 100$ trials of data over $N = 100$ discretization points. Dashed lines are true values, solid lines are estimates and shaded regions are 95% credible bands.

F.3. Scalability of Dynamical Covariance Model

Now we use the same simulation model (16) for $D = 100$ dimensions to test the scalability of our dynamic model (8). However instead of the full covariance, we only consider a diagonal covariance matrix plus 4 non-zero off-diagonal entries $\sigma_{1,2}$ ($\sigma_{2,1}$) and $\sigma_{99,100}$ ($\sigma_{100,99}$). We focus on the correlation process in this example thus set $\mu_t \equiv 0$ and $\sigma_t \equiv 1$, for $t \in [0, 1]$. More specifically when generating data $\{y_t\}$ with (16), if $i \notin \{2, 100\}$ we set i -th rows $L_i = S_i = e_i$ with e_i being the i -th row of identity matrix.

To apply our dynamical model (8) in this setting, we let \mathbf{L}_t have ‘ w -band’ structure with $w = 2$ at each time t . Setting $s = 2$, $a = 1$, $b = 0.1$, $m = 0$ and $V = 10^{-3}$, $N = 100$ and $M = 100$, we repeat the MCMC runs for 7.5×10^4 iterations, burn in the first 2.5×10^4 and subsample 1 for every 10 to obtain 5×10^3 posterior samples in the end. Based on those samples, we estimate the underlying correlation functions and only plot $\rho_{1,2}$, $\rho_{49,50}$ and $\rho_{99,100}$ in Figure F.5. With the ‘ w -band’ structure, we have less entries in the covariance matrix and focus on the ‘in-group’ correlation. Our dynamical model (8) is sensitive enough to discern the informative non-zero components from the non-informative ones in these correlation functions. Unit-vector GP priors provide flexibility for the model to capture the changing pattern of informative correlations. The left panel of Figure F.5 shows that the model (8) correctly identify the non-zero components $\rho_{1,2}$ and $\rho_{99,100}$ and characterize their evolution. The right panel shows that the 2-norm distance between the estimated and true correlation matrices, $\|\hat{P}(t) - P(t)\|_2$, is small, indicating that our dynamic model (8) performs well with higher dimension in estimating complex dependence structure among multiple stochastic processes.

F.4. More Results on the Analysis of LFP data

In Section 5, we studied the LFP data collected from the hippocampus of rats performing a complex sequence memory task. Figure F.6 shows 12 locations from CA1 subregion of the hippocampus of the rat where LFP signals are recorded. Figure F.7 shows $M = 20$ trials of these LFP signals from $D = 4$ channels under both InSeq and OutSeq conditions. Figure F.8 shows the theta-filtered traces (4-12Hz; left panel) and the estimated correlation processes under different experiment conditions (InSeq vs OutSeq; right panel). Here we observe a similar dynamic pattern of correlation matrices under two conditions that diverge after 500ms, indicating the neural activity associated with the cognitive process of identifying whether events occurred in their expected order.

We also did a study of the correlation evolution on the full 12 channels and revealed the block structure of those channels and the same changing pattern under different experimental conditions discovered with the chosen 4 channels in Section 5. This video demonstrates the result of 12 channels <https://www.youtube.com/watch?v=NMUUic0IDsm>.

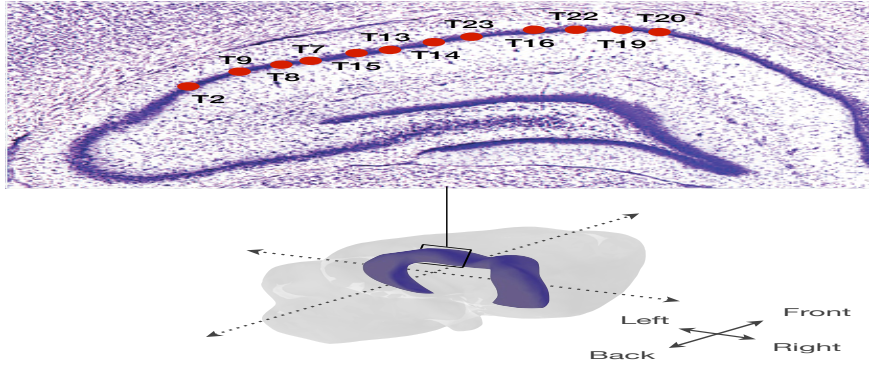


Fig. F.6: Locations of recorded LFP signals in CA1 subregion of the rat’s hippocampus.

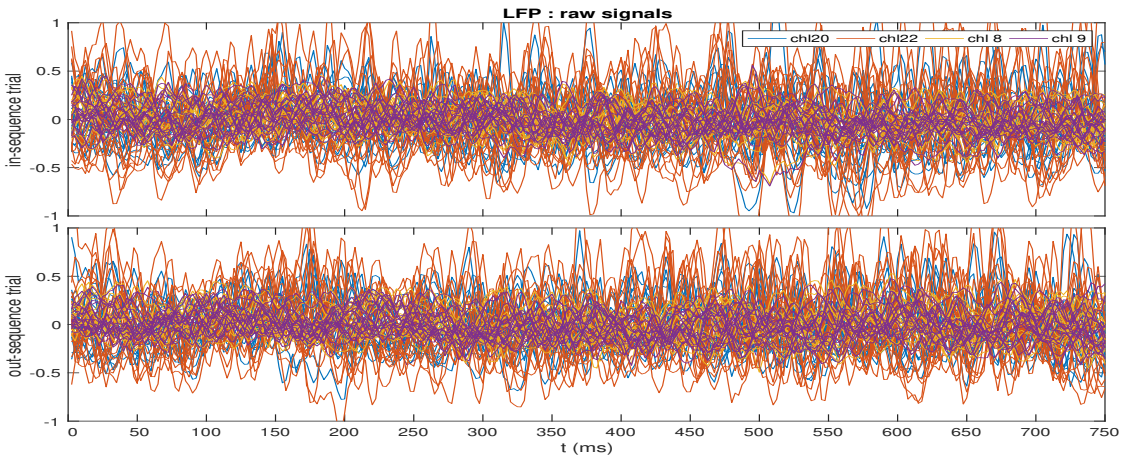


Fig. F.7: LFP signals on “in sequence” and “out of sequence” trials. It is difficult to identify differences between the two conditions based on a mere visual inspection of the LFPs.

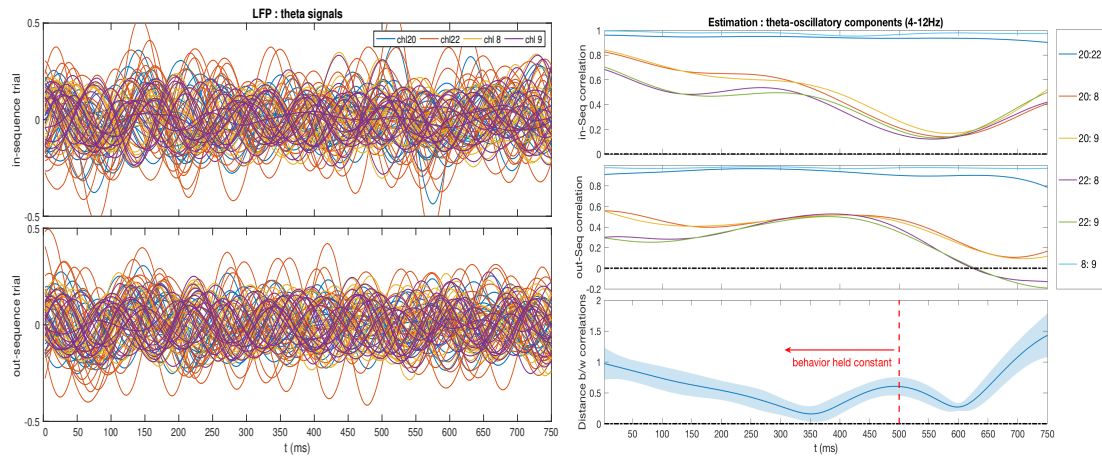


Fig. F.8: Results of LFP theta signals: data (left), estimation of correlations (right).

REFERENCES

- ALLEN, T. A., MORRIS, A. M., MATTFELD, A. T., STARK, C. E. & FORTIN, N. J. (2014). A sequence of events model of episodic memory shows parallels in rats and humans. *Hippocampus* **24**, 1178–1188.
- ALLEN, T. A., SALZ, D. M., MCKENZIE, S. & FORTIN, N. J. (2016). Nonspatial sequence coding in ca1 neurons. *Journal of Neuroscience* **36**, 1547–1563.
- ANDERSON, T. W. (2003). *An Introduction to Multivariate Statistical Analysis*. Wiley Series in Probability and Statistics. Hoboken, N. J.: Wiley Interscience.
- BANFIELD, J. D. & RAFTERY, A. E. (1993). Model-based gaussian and non-gaussian clustering. *Biometrics* , 803–821.
- BARNARD, J., MCCULLOCH, R. & MENG, X.-L. (2000). Modeling covariance matrices in terms of standard deviations and correlations, with application to shrinkage. *Statistica Sinica* , 1281–1311.
- BENSMAIL, H., CELEUX, G., RAFTERY, A. E. & ROBERT, C. P. (1997). Inference in model-based cluster analysis. *statistics and Computing* **7**, 1–10.
- BESKOS, A., PINSKI, F. J., SANZ-SERNA, J. M. & STUART, A. M. (2011). Hybrid monte carlo on hilbert spaces. *Stochastic Processes and their Applications* **121**, 2201–2230.
- BINGHAM, C. (1974). An antipodally symmetric distribution on the sphere. *The Annals of Statistics* , 1201–1225.
- CELEUX, G. & GOVAERT, G. (1995). Gaussian parsimonious clustering models. *Pattern recognition* **28**, 781–793.
- CHIU, T. Y., LEONARD, T. & TSUI, K.-W. (1996). The matrix-logarithmic covariance model. *Journal of the American Statistical Association* **91**, 198–210.
- CHO, H. & FRYZLEWICZ, P. (2015). Multiple-change-point detection for high dimensional time series via sparsified binary segmentation. *Journal of the Royal Statistical Society: Series B (Statistical Methodology)* **77**, 475–507.
- CLAUSEN, T. (1832). Über die Function $\sin \phi + (1/2^2) \sin 2\phi + (1/3^2) \sin 3\phi + \text{etc.}$ *Journal für die reine und angewandte Mathematik* **8**, 298–300.
- CRIBBEN, I., HARALDSDOTTIR, R., ATLAS, L. Y., WAGER, T. D. & LINDQUIST, M. A. (2012). Dynamic connectivity regression: Determining state-related changes in brain connectivity. *NeuroImage* **61**, 907 – 920.
- DAHLHAUS, R. (2000). A likelihood approximation for locally stationary processes. *Ann. Statist.* **28**, 1762–1794.
- DANIELS, M. J. (1999). A prior for the variance in hierarchical models. *Canadian Journal of Statistics* **27**, 567–578.
- DANIELS, M. J. & KASS, R. E. (1999). Nonconjugate bayesian estimation of covariance matrices and its use in hierarchical models. *Journal of the American Statistical Association* **94**, 1254–1263.
- DANIELS, M. J. & KASS, R. E. (2001). Shrinkage estimators for covariance matrices. *Biometrics* **57**, 1173–1184.
- DUANE, S., KENNEDY, A. D., PENDLETON, B. J. & ROWETH, D. (1987). Hybrid Monte Carlo. *Physics Letters B* **195**, 216 – 222.
- FIECAS, M. & OUBAO, H. (2016). Modeling the evolution of dynamic brain processes during an associative learning experiment. *Journal of the American Statistical Association* **111**, 1440–1453.
- FISHER, N. I., LEWIS, T. & EMBLETON, B. J. (1987). *Statistical analysis of spherical data*. Cambridge university press.
- FISHER, R. (1953). Dispersion on a sphere. In *Proceedings of the Royal Society of London A: Mathematical, Physical and Engineering Sciences*, vol. 217. The Royal Society.
- FOX, E. B. & DUNSON, D. B. (2015). Bayesian nonparametric covariance regression. *Journal of Machine Learning Research* **16**, 2501–2542.
- GHOSAL, S., GHOSH, J. K. & VAN DER VAART, A. W. (2000). Convergence rates of posterior distributions. *Ann. Statist.* **28**, 500–531.
- GIROLAMI, M. & CALDERHEAD, B. (2011). Riemann manifold Langevin and Hamiltonian Monte Carlo methods. *Journal of the Royal Statistical Society, Series B (with discussion)* **73**, 123–214.
- HOFFMAN, M. D. & GELMAN, A. (2014). The no-u-turn sampler: Adaptively setting path lengths in hamiltonian monte carlo. *The Journal of Machine Learning Research* **15**, 1593–1623.
- HOLBROOK, A., LAN, S., VANDENBERG-RODES, A. & SHAHBABA, B. (2016). Geodesic lagrangian monte carlo over the space of positive definite matrices: with application to bayesian spectral density estimation. *arXiv preprint arXiv:1612.08224* .
- HOLBROOK, A., VANDENBERG-RODES, A., FORTIN, N. & SHAHBABA, B. (2017). A bayesian supervised dual-dimensionality reduction model for simultaneous decoding of lfp and spike train signals. *Stat* **6**, 53–67. Sta4.137.
- KENT, J. T. (1982). The fisher-bingham distribution on the sphere. *Journal of the Royal Statistical Society. Series B (Methodological)* , 71–80.
- LAN, S. & SHAHBABA, B. (2016). *Algorithmic Advances in Riemannian Geometry and Applications*, chap. 2. Advances in Computer Vision and Pattern Recognition. Springer International Publishing, 1st ed., pp. 25–71.
- LAN, S., ZHOU, B. & SHAHBABA, B. (2014). Spherical hamiltonian monte carlo for constrained target distributions. vol. 32. The 31st International Conference on Machine Learning, Beijing.
- LEONARD, T. & HSU, J. S. (1992). Bayesian inference for a covariance matrix. *The Annals of Statistics* , 1669–1696.
- LIECHTY, J. C. (2004). Bayesian correlation estimation. *Biometrika* **91**, 1–14.
- LINDQUIST, M. A., XU, Y., NEBEL, M. B. & CAFFO, B. S. (2014). Evaluating dynamic bivariate correlations in resting-state fmri: A comparison study and a new approach. *NeuroImage* **101**, 531 – 546.

- LIU, C. (1993). Bartlett's decomposition of the posterior distribution of the covariance for normal monotone ignorable missing data. *Journal of Multivariate Analysis* **46**, 198–206.
- MAGNUS, J. R. & NEUDECKER, H. (1979). The commutation matrix: some properties and applications. *The Annals of Statistics*, 381–394.
- MAGNUS, J. R. & NEUDECKER, H. (1980). The elimination matrix: some lemmas and applications. *SIAM Journal on Algebraic Discrete Methods* **1**, 422–449.
- MARDIA, K. V. & JUPP, P. E. (2009). *Directional statistics*, vol. 494. John Wiley & Sons.
- MARDIA, K. V., KENT, J. T. & BIBBY, J. M. (1980). *Multivariate analysis (probability and mathematical statistics)*. MINKA, T. (1997; revised 12/00). *Old and New Matrix Algebra Useful for Statistics*. MIT Media Lab note.
- MURRAY, I., ADAMS, R. P. & MACKAY, D. J. (2010). Elliptical slice sampling. *JMLR: W&CP* **9**, 541–548.
- NASON, G. P., VON SACHS, R. & KROISANDT, G. (2000). Wavelet processes and adaptive estimation of the evolutionary wavelet spectrum. *Journal of the Royal Statistical Society: Series B (Statistical Methodology)* **62**, 271–292.
- NEAL, R. M. (2003). Slice sampling. *Annals of Statistics* **31**, 705–767.
- NEAL, R. M. (2011). MCMC using Hamiltonian dynamics. In *Handbook of Markov Chain Monte Carlo*, S. Brooks, A. Gelman, G. Jones & X. L. Meng, eds. Chapman and Hall/CRC, pp. 113–162.
- NESTEROV, Y. (2009). Primal-dual subgradient methods for convex problems. *Mathematical programming* **120**, 221–259.
- NG, C.-W., ELIAS, G. A., ASEM, J. S., ALLEN, T. A. & FORTIN, N. J. (2017). Nonspatial sequence coding varies along the cal transverse axis. *Behavioural Brain Research*.
- OMBAO, H., VON SACHS, R. & GUO, W. (2005). Slex analysis of multivariate nonstationary time series. *Journal of the American Statistical Association* **100**, 519–531.
- ONSTOTT, T. C. (1980). Application of the bingham distribution function in paleomagnetic studies. *Journal of Geophysical Research: Solid Earth* **85**, 1500–1510.
- PARK, T., ECKLEY, I. A. & OMBAO, H. C. (2014). Estimating time-evolving partial coherence between signals via multivariate locally stationary wavelet processes. *IEEE Transactions on Signal Processing* **62**, 5240–5250.
- PINHEIRO, J. C. & BATES, D. M. (1996). Unconstrained parametrizations for variance-covariance matrices. *Statistics and Computing* **6**, 289–296.
- POURAHMADI, M. (1999). Joint mean-covariance models with applications to longitudinal data: Unconstrained parameterisation. *Biometrika*, 677–690.
- POURAHMADI, M. (2000). Maximum likelihood estimation of generalised linear models for multivariate normal covariance matrix. *Biometrika*, 425–435.
- POURAHMADI, M. & WANG, X. (2015). Distribution of random correlation matrices: Hyperspherical parameterization of the cholesky factor. *Statistics & Probability Letters* **106**, 5 – 12.
- PRADO, R. (2013). Sequential estimation of mixtures of structured autoregressive models. *Computational Statistics & Data Analysis* **58**, 58 – 70. The Third Special Issue on Statistical Signal Extraction and Filtering.
- PRIESTLEY, M. (1965). Evolutionary and non-stationary processes. *J. Roy. Statist. Soc. Ser. B* **27**, 204–237.
- RAPISARDA, F., BRIGO, D. & MERCURIO, F. (2007). Parameterizing correlations: a geometric interpretation. *IMA Journal of Management Mathematics* **18**, 55–73.
- SMITH, W. & HOCKING, R. (1972). Algorithm as 53: Wishart variate generator. *Journal of the Royal Statistical Society. Series C (Applied Statistics)* **21**, 341–345.
- SVERDRUP, E. (1947). Derivation of the wishart distribution of the second order sample moments by straightforward integration of a multiple integral. *Scandinavian Actuarial Journal* **1947**, 151–166.
- TING, C. M., SEGHOUEANE, A. K., SALLEH, S. H. & NOOR, A. M. (2015). Estimating effective connectivity from fmri data using factor-based subspace autoregressive models. *IEEE Signal Processing Letters* **22**, 757–761.
- TOKUDA, T., GOODRICH, B., VAN MECHELEN, I., GELMAN, A. & TUERLINCKX, F. (2011). Visualizing distributions of covariance matrices. *Columbia Univ., New York, USA, Tech. Rep*, 18–18.
- TRACY, D. S. & DWYER, P. S. (1969). Multivariate maxima and minima with matrix derivatives. *Journal of the American Statistical Association* **64**, 1576–1594.
- VAN DER VAART, A. & VAN ZANTEN, H. (2011). Information rates of nonparametric gaussian process methods. *J. Mach. Learn. Res.* **12**, 2095–2119.
- VAN DER VAART, A. W. & VAN ZANTEN, J. H. (2008a). Rates of contraction of posterior distributions based on gaussian process priors. *The Annals of Statistics* **36**, 1435–1463.
- VAN DER VAART, A. W. & VAN ZANTEN, J. H. (2008b). *Reproducing kernel Hilbert spaces of Gaussian priors*, vol. Volume 3 of *Collections*. Beachwood, Ohio, USA: Institute of Mathematical Statistics, pp. 200–222.
- VAN DER VAART, A. W. & VAN ZANTEN, J. H. (2009). Adaptive bayesian estimation using a gaussian random field with inverse gamma bandwidth. *Ann. Statist.* **37**, 2655–2675.
- WILSON, A. G. & GHAHRAMANI, Z. (2011). Generalised wishart processes. In *Proceedings of the 27th Conference on Uncertainty in Artificial Intelligence*.
- WISHART, J. (1928). The generalised product moment distribution in samples from a normal multivariate population. *Biometrika*, 32–52.

- YANG, R. & BERGER, J. O. (1994). Estimation of a covariance matrix using the reference prior. *The Annals of Statistics* , 1195–1211.
- YANG, Y. & DUNSON, D. B. (2016). Bayesian manifold regression. *Ann. Statist.* **44**, 876–905.

[Received XX XXX XXXX. Editorial decision on XX XXX XXXX]